Combustion and Flame 157 (2010) 1833–1849

Contents lists available at ScienceDirect

Combustion and Flame

journal homepage: www.elsevier.com/locate/combustflame

Coupling of the model reduction technique with the lattice Boltzmann method for combustion simulations

Eliodoro Chiavazzo [a,b,*], Iliya V. Karlin [a,c], Alexander N. Gorban [d], Konstantinos Boulouchos [a]

[a] Aerothermochemistry and Combustion Systems Lab, ETH Zurich, 8092 Zurich, Switzerland
[b] Department of Energetics, Politecnico di Torino, Corso Duca degli Abruzzi 24, 10129 Turin, Italy
[c] School of Engineering Sciences, University of Southampton, SO17 1BJ Southampton, UK
[d] Department of Mathematics, University of Leicester, LE1 7RH Leicester, UK

ARTICLE INFO

Article history:
Received 17 June 2009
Received in revised form 30 March 2010
Accepted 17 June 2010
Available online 14 July 2010

Keywords:
Combustion
Model reduction
Invariant manifold
Lattice Boltzmann method

ABSTRACT

A new framework of simulation of reactive flows is proposed based on a coupling between accurate reduced reaction mechanism and the lattice Boltzmann representation of the flow phenomena. The model reduction is developed in the setting of slow invariant manifold construction, and the simplest lattice Boltzmann equation is used in order to work out the procedure of coupling of the reduced model with the flow solver. Practical details of constructing slow invariant manifolds of a reaction system under various thermodynamic conditions are reported. The proposed method is validated with the two-dimensional simulation of a premixed counterflow flame in the hydrogen-air mixture.

1. Introduction

Accurate modeling of reactive flows requires the solution of a large number of conservation equations as dictated by detailed reaction mechanism. In addition to the sometimes prohibitively large number of variables introduced, the numerical solution of the governing equations has to face the stiffness due to disparate time scales of the kinetic terms. These issues make computations of even simple flames time consuming, and have particularly negative impact on the lattice Boltzmann method [31,32], whose number of fields (distribution functions or populations) may be significantly larger than the number of conventional fields (density, momenta, temperature, species mass fractions). The lattice Boltzmann (LB) method is a relatively novel approach to numerical flow simulations, and recent studies have proved that it is competitive to traditional methods when simulating compressible [28] and turbulent flows [29] in terms of both accuracy and efficiency. Although this makes LB a good candidate for computing reactive flows, applications in this field are still limited by the stiffness of the governing equations and the large number of fields to solve.

On the other hand, the difference of time scales can be exploited in order to construct a reduced description of the detailed model. In fact, because of the stiffness, the dynamics of homogeneous reactive systems is often characterized by a short transient towards a low dimensional manifold in the concentration space, known as the *slow invariant manifold* (SIM). The subsequent dynamics is slower and it proceeds along the manifold itself, until a steady state is reached. Constructing such manifolds can lead to a simpler and less stiff description of the reactive system, where the fast transient is neglected and the slow dynamics can be reproduced with high accuracy. Therefore, much effort has been devoted to achieving that aim; the intrinsic low dimensional manifold (ILDM) approach [35], the computational singular perturbation (CSP) method [36] and the Flamelet-Generated Manifolds (FGM) method [22,23] are representative examples.

In this work, we make use of the method of invariant grids (MIG) [1–3] which is also based on the notion of SIM, and it has been recently elaborated for combustion applications [8,9] with the aim of automating the model reduction procedure. In particular, its realization follows two key steps. First, an initial rough reduced description of the complex chemical mechanism is constructed making use of the notion of *quasi equilibrium manifold* (QEM). Second, the latter initial approximation is iteratively refined until the *invariant grid* is constructed. Finally, we employ the reduced model of the hydrogen mechanism in a lattice Boltzmann code for simulating laminar flames throughout a homogeneous mixture.

This paper is organized in sections as follows. In Section 2, the kinetic equation for a batch reactor is reviewed. The construction of a reduced model using the method of invariant grids is briefly

* Corresponding author at: Department of Energetics, Politecnico di Torino, Corso Duca degli Abruzzi 24, 10129 Turin, Italy. Fax: +39 011 564 4499.
E-mail addresses: eliodoro.chiavazzo@gmail.com (E. Chiavazzo), karlin@lav.mavt.ethz.ch (I.V. Karlin), ag153@leicester.ac.uk (A.N. Gorban), boulouchos@lav.mavt.ethz.ch (K. Boulouchos).

0010-2180/$ - see front matter © 2010 The Combustion Institute. Published by Elsevier Inc. All rights reserved.
doi:10.1016/j.combustflame.2010.06.009

described in Section 3. In Section 4, the lattice Boltzmann method for reactive flows is reviewed, and the coupling with a reduced model is presented in Section 4.2. Results are discussed in Section 5. A detailed discussion on the construction of thermodynamic Lyapunov functions, and on the exact computation of their derivatives (as requested in order to implement the MIG to combustion applications) is presented in Appendix A. Finally, the exact evaluation of the Jacobian matrix of a system of kinetic equations is addressed in the Appendix B.

2. Detailed reaction kinetics in a batch reactor

In this section, we focus on homogeneous mixtures of ideal gases reacting in a closed system. Let $x_1,\dots,x_n$ be n chemical species participating in a detailed reaction mechanism with r reversible steps

$$\nu'_{s1}x_1+\cdots+\nu'_{sn}x_n \rightleftharpoons \nu''_{s1}x_1+\cdots+\nu''_{sn}x_n, \quad s=1,\dots,r, \tag{1}$$

where ν'_{si} and ν''_{si} are the stoichiometric coefficients of species i in the reaction step s for reactants and products. Let the stoichiometric vectors be $\boldsymbol{\nu}'_s=(\nu'_{s1},\dots,\nu'_{sn})$, $\boldsymbol{\nu}''_s=(\nu''_{s1},\dots,\nu''_{sn})$ and $\boldsymbol{\nu}_s=\boldsymbol{\nu}''_s-\boldsymbol{\nu}'_s$. The reaction rate of step s reads

$$\begin{aligned}&\Omega_s=\Omega_s^+-\Omega_s^-,\\ &\Omega_s^+=k_s^+(T)\prod_{i=1}^n c_i^{\alpha_i}, \quad \Omega_s^-=k_s^-(T)\prod_{i=1}^n c_i^{\beta_i}.\end{aligned} \tag{2}$$

Let N_i and V be the mole number of species i and the reactor volume, respectively, the corresponding molar concentration is given by $c_i=N_i/V$. The forward and reverse reaction rate constants k_s^+, k_s^- take the Arrhenius form

$$k_s(T)=A_sT^{\beta_s}\exp\left(\frac{-E_{as}}{\mathscr{R}T}\right), \tag{3}$$

where A_s denotes the pre-exponential factor, β_s the temperature exponent, E_{as} the activation energy of reaction s and $\mathscr{R}$ is the universal gas constant. The rate of change of species i is given by

$$\dot{\omega}_i=\sum_{s=1}^r \boldsymbol{\nu}_s(i)\Omega_s, \quad i=1,\dots,n, \tag{4}$$

with forward and reverse reaction rate constants related by the equilibrium constant $K_{c,s}=k_s^+/k_s^-$, which can be obtained by imposing the *principle of detail balance* at the steady state:

$$\Omega_s^+=\Omega_s^-, \quad s=1,\dots,r. \tag{5}$$

In the following, an arbitrary point of the composition space will be denoted by $\boldsymbol{c}=(c_1,\dots,c_n)$, where c_i is the molar concentration of species i. Moreover, a given state of a homogeneous ideal gas mixture is fully described by a vector $\boldsymbol{c}$ and one independent *intensive* property, e.g., the corresponding temperature T. An alternative description of the system is also given by $\boldsymbol{\psi}=(Y_1,\dots,Y_n)$ and two independent intensive properties, e.g., temperature T and total pressure p, where Y_i is the mass fraction of species i.

Under isochoric and isothermal conditions (V, $T=const$), the reaction kinetic Eq. (4) are closed, and the temporal evolution of the species concentrations in the reactor obeys the following system of ordinary differential equations:

$$\frac{d\boldsymbol{c}}{dt}=(\dot{\omega}_1,\dots,\dot{\omega}_n)^T=\boldsymbol{f}, \tag{6}$$

whereas, for different cases, additional closure relations are needed. Two cases are relevant to combustion: isolated reactor with constant volume and mixture-averaged internal energy ($V,\overline{U}=const$), and thermal isolated isobaric reactor with constant total pressure and mixture-averaged enthalpy ($p,\bar{h}=const$). In the first case, the governing equations read

$$\begin{aligned}&\overline{U}=\sum_{i=1}^n U_i(T)Y_i=const,\\ &\frac{d\boldsymbol{c}}{dt}=(\dot{\omega}_1,\dots,\dot{\omega}_n)^T=\boldsymbol{f},\end{aligned} \tag{7}$$

where for each species i, the temperature dependence of the specific internal energy U_i is taken into account by a polynomial fit

$$U_i(T)=\mathscr{R}\left(a_{1i}T+\frac{a_{2i}}{2}T^2+\frac{a_{3i}}{3}T^3+\frac{a_{4i}}{4}T^4+\frac{a_{5i}}{5}T^5+a_{6i}\right)-\mathscr{R}T. \tag{8}$$

Here, following [42], the temperature dependence of thermodynamic properties of species i are expressed in terms of tabulated constants a_{ji}, with $j=1,\dots,7$.

Let W_i be the molecular weight of species i, for closed reactors under fixed total pressure and mixture-averaged enthalpy, the dynamics of the mass fractions Y_i obeys the following equation system

$$\begin{aligned}&\bar{h}=\sum_{i=1}^n h_i(T)Y_i=const,\\ &c_i=\frac{p(Y_i/W_i)}{\mathscr{R}T\sum_{j=1}^n Y_j/W_j},\\ &\frac{d\boldsymbol{\psi}}{dt}=\left(\frac{W_1\dot{\omega}_1}{\bar{\rho}},\dots,\frac{W_n\dot{\omega}_n}{\bar{\rho}}\right)^T=\boldsymbol{f},\end{aligned} \tag{9}$$

where the mixture density $\bar{\rho}$ and the specific enthalpy h_i of species i take the explicit form

$$\bar{\rho}=\sum_{i=1}^n W_ic_i, \quad h_i(T)=U_i(T)+\mathscr{R}T. \tag{10}$$

Notice that, for non-isothermal cases, the temperature corresponding to the composition state $\boldsymbol{\psi}$ is not explicitly known. Therefore, the right-hand side of (4) can be evaluated after solving the two energy conservation equations in (7) and (9) with respect to T (e.g., using the Newton–Raphson method).

Finally, in a closed chemically reactive system, the atom mole numbers N_k of each element k must be conserved:

$$\boldsymbol{D}\boldsymbol{\psi}^T=(N_1,\dots,N_d)^T, \quad \frac{dN_k}{dt}=0, \quad \boldsymbol{D}(k,i)=\frac{\mu_{ik}}{W_i}, \tag{11}$$

where μ_{ik} is the number of atoms of the kth element in species i, and $\boldsymbol{D}$ is a $(d\times n)$ matrix, while d is the number of elements involved in the reaction. In other words, the vector field $\boldsymbol{f}$ of motions in the phase-space is always orthogonal (in Euclidean sense) to the rows of $\boldsymbol{D}$.

The interested reader is delegated to the classical work of Williams [40] for a detailed discussion on the theory of chemical kinetics.

3. Reduced description

In our study, the detailed mechanism of Li et al. [4] (9 species, 21 elementary reactions) for hydrogen combustion is considered, and we search for a reduced description with two degrees of freedom. Here, we present a general overview of the method of invariant grids (MIG) for model reduction in chemical kinetics. The interested reader can find more details in Refs. [1,2,6–9].

3.1. Initial approximation: quasi equilibrium manifold

Approximated reduced descriptions in chemical kinetics can be based on the notion of quasi equilibrium manifold [1,2]. Hence, let us construct a quasi equilibrium manifold for a stoichiometric H_2-air mixture under fixed pressure $p=1$ bar and enthalpy $\bar{h}=2.8$ kJ/kg, corresponding to the temperature $T_0=300$ K for the stoichiometric unburned mixture $H_2+0.5O_2+1.88N_2$. A generic $q-$dimensional QEM is obtained by solving the following minimization problem:

$$\begin{cases} G \to \min \\ \sum_i m_j^i Y_i = \xi^j, \quad j = 1, \ldots, q. \end{cases} \tag{12}$$

Here, G represents a thermodynamic Lyapunov function with respect to the kinetic Eq. (4), whose construction is discussed in detail in Appendix A. The vector set $\left\{\boldsymbol{m}_j = \left(m_j^1, \ldots, m_j^9\right)\right\}$ is used to re-parameterize the mass fractions Y_i in terms of new variables ξ^j, which are expected to follow a slow dynamics. Several suggestions for defining slow lumped variables in chemical kinetics can be found in the literature, and for our purposes here we use a 2-dimensional manifold parameterized by the *total number of moles* ξ^1 and the *free oxygen* ξ^2, respectively (see, e.g., [5]):

$$\xi^1 = \sum_{i=1}^{9} \frac{Y_i}{W_i}, \quad \xi^2 = \frac{Y_O}{W_O} + \frac{Y_{OH}}{W_{OH}} + \frac{Y_{H_2O}}{W_{H_2O}}. \tag{13}$$

It is worth stressing that, when searching for a QEM as a reduced description of a detailed model in combustion problems, the parameters ξ^i in (12) are assumed to be *slow variables*. The choice of the latter variables is crucial since it affects the accuracy of the QEM in describing the corresponding SIM. In this study, the chosen parameters ξ^i (13) are referred to as slow variables because we make use of the Rate Controlled Constrained Equilibrium (RCCE) parameterization [10], where the ξ^i are directly linked to slow physical quantities. In particular, ξ^1 is typically termed the total number of moles and is expected to (globally) follow a slow dynamics due to the slow recombination/dissociation reactions. On the other hand, the free oxygen ξ^2 (linked to the species with any oxygen which is not bonded to another oxygen) is imposed by reactions where the O–O bond is broken. A more general discussion on the RCCE constraints, can be found in the literature [11]. Note that, a different systematic parameterization of quasi equilibrium manifolds was also introduced recently [7], where the vectors $\boldsymbol{m}_j$ are defined on the basis of the eigenvectors of the Jacobian matrix $\boldsymbol{J} = [\partial f_i/\partial Y_j]$ evaluated at the steady state $\boldsymbol{c}^{eq}$. In this case, it can be shown that the QEM is tangent to the corresponding SIM at $\boldsymbol{c}^{eq}$ (see Refs. [6,7]), proving that the chosen parameters are slow variables at least in a vicinity of $\boldsymbol{c}^{eq}$. The latter will be referred to as *spectral quasi equilibrium manifold* (SQEM) parameterization. It is worth stressing that, although the choice of the parameterization vectors affects the accuracy of a quasi equilibrium manifold in describing the corresponding SIM, solutions of (12) are anyway refined and the final result does not depend on the initial approximation (and parameterization) (see also Section 3.2). Finally, notice that below we deal with discrete representations of manifolds: *grids*. A grid consists of a set of nodes in the concentration space and connections between them, that enable to define the grid tangent space at each node.

In particular, in the following we review the quasi equilibrium grid algorithm [6] for constructing discrete approximation of a QEM. Let $\boldsymbol{E}$ be the $(d+q)\times n$ matrix, obtained by adding the $\boldsymbol{m}_j$ vectors as q additional rows to the matrix $\boldsymbol{D}$. Let the steady state of (9) be denoted by $\boldsymbol{c}^0 = (c_1^0, \ldots, c_n^0)$. The QEM state $\boldsymbol{c}^1$ can be computed, in a neighborhood of $\boldsymbol{c}^0$, by solving the linear algebraic system

$$\begin{aligned} &\sum_{i=1}^{z} \left(\boldsymbol{t}_j \boldsymbol{H} \boldsymbol{\rho}_i^T\right)\varphi_i = -\boldsymbol{t}_j \nabla G^T, \quad j = 1, \ldots, z-q, \\ &\sum_{i=1}^{z} \left(\boldsymbol{m}_1 \boldsymbol{\rho}_i^T\right)\varphi_i = 0, \\ &\vdots \\ &\sum_{i=1}^{z} \left(\boldsymbol{m}_k \boldsymbol{\rho}_i^T\right)\varphi_i = \varepsilon_k, \\ &\vdots \\ &\sum_{i=1}^{z} \left(\boldsymbol{m}_q \boldsymbol{\rho}_i^T\right)\varphi_i = 0, \end{aligned} \tag{14}$$

with respect to the unknowns φ_i, where ∇G and $\boldsymbol{H}$ are the gradient and the second derivative matrix of G, respectively (the explicit computation of those derivatives is given in Appendix A). If $\{\boldsymbol{\rho}_1, \ldots, \boldsymbol{\rho}_z\}$ and $\{\boldsymbol{t}_1, \ldots, \boldsymbol{t}_{z-q}\}$ are two vector bases spanning the null space of the matrix $\boldsymbol{D}$ and $\boldsymbol{E}$, respectively, then

$$\begin{aligned} &\boldsymbol{c}^1 = (c_1^0 + dc_1, \ldots, c_n^0 + dc_n), \\ &(dc_1, \ldots, dc_n) = \sum_{i=1}^{z} \varphi_i \boldsymbol{\rho}_i. \end{aligned} \tag{15}$$

By referring to system (14), all derivatives of G are evaluated at $\boldsymbol{c}^0$ and, through the last q equations, we impose that $\boldsymbol{c}^1$ belongs to a Cartesian grid in the space $\{\xi^1, \ldots, \xi^q\}$, with the fixed parameter ε_k defining the grid step along ξ^k. Similarly, by solving (14) at $\boldsymbol{c}^1$, a new QEM point $\boldsymbol{c}^2$ can be found. In general, this procedure can be iterated as long as all the coordinates of the computed state remain non-negative. In the following, we refer to the collection of computed states as *quasi equilibrium grid*. An approximated solution to (12), computed making use of the above algorithm, is shown in Fig. 1, where $q = 2$ and $\varepsilon_1 = \varepsilon_2 = 1.8 \times 10^{-4}$.

3.2. Grid refinement and invariant grids

An arbitrary quasi equilibrium grid $\mathscr{G}$ is defined by a mapping $\boldsymbol{c} = F(\xi^1, \ldots, \xi^q)$ of a discrete subset of the parameter space into the concentration space. According to MIG, the reduced description of a batch reactor is given by the corresponding *invariant grid*, which is the *stable fixed point* of the relaxation of a QEG $\mathscr{G}$ under the following film equation of dynamics [1]

$$\frac{d\mathscr{G}}{dt} = \boldsymbol{f} - \boldsymbol{P}\boldsymbol{f}, \tag{16}$$

where $\boldsymbol{f}$ and $\boldsymbol{P}$ denote the vector of motion in the phase-space and a projector operator onto the grid tangent space T_ξ, respectively. Defining $\boldsymbol{P}$ on a grid requires a smooth continuation of the discrete mapping F on the parameter space: To this end, low-order interpolation schemes can be successfully adopted in order to compute local tangent vectors [8]. In this work, the independent vectors $\hat{\boldsymbol{u}}_j$ spanning T_ξ are approximated with second-order accurate finite differences, and grid refinement is addressed using an explicit low-order numerical scheme for integrating the film Eq. (16). Namely, at each iteration, all grid nodes $\boldsymbol{c}$ are shifted by the amount $\delta\boldsymbol{c}$ such that the updated nodes are $\boldsymbol{c} + \delta\boldsymbol{c}$ with

$$\delta\boldsymbol{c} = \vartheta(\boldsymbol{f}(\boldsymbol{c}) - \boldsymbol{P}\boldsymbol{f}(\boldsymbol{c})). \tag{17}$$

The parameter ϑ has the dimension of time, and its estimate can be found in the literature [2]:

$$\vartheta = \frac{\boldsymbol{\Delta}\boldsymbol{H}\boldsymbol{\Delta}^T}{\boldsymbol{\Delta}\boldsymbol{H}\boldsymbol{J}'\boldsymbol{\Delta}^T}, \tag{18}$$

where $\boldsymbol{\Delta}$ is the *defect of invariance* and it is defined by the right-hand side of (16), while $\boldsymbol{J}'$ is the symmetric part of the Jacobian matrix $\boldsymbol{J} = [\partial f_i/\partial Y_j]$ as discussed in Appendix B. The convergence criterion is based on a comparison of the Euclidean norm of defect of invariance $|\boldsymbol{\Delta}|$ against the norm of vector field $|\boldsymbol{f}|$ [7]. In particular, here iterations are terminated when at all nodes the following inequality holds: $|\boldsymbol{\Delta}|/|\boldsymbol{f}| \leqslant 0.01$. Whenever the latter ratio keeps increasing during refinement, the corresponding grid node is discarded. The projector $\boldsymbol{P}$ is constructed as discussed in Section 3.4. The 2-dimensional refined grid is shown in Fig. 2, and it is compared to the initial quasi equilibrium grid in Fig. 3.

Notice that in the low-temperature region ($T < 800$ K), the invariant grid is not convergent, meaning that a 2-dimensional reduced description is not sufficient and the dimension of the slow invariant manifold is larger than two.

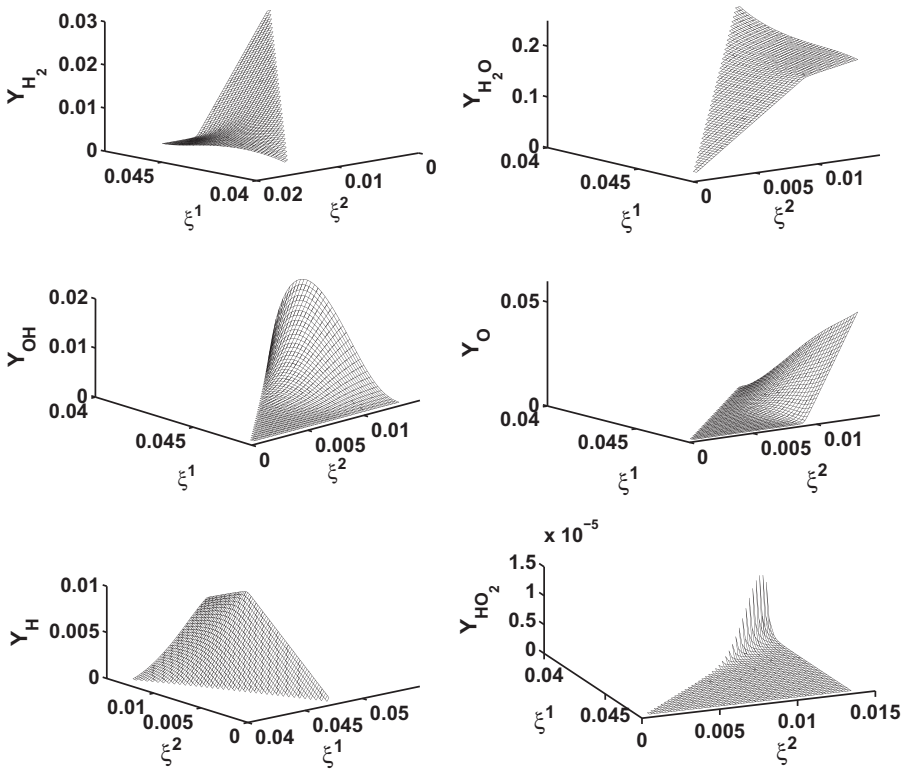

Fig. 1. 2-dimensional quasi equilibrium grid (QEG) for stoichiometric mixture of hydrogen and air, under $p = 1$ bar and $\bar{h} = 2.8$ kJ/kg. Six coordinates function of the parameters ξ^1, ξ^2 with $\varepsilon_1 = \varepsilon_2 = 1.8 \times 10^{-4}$.

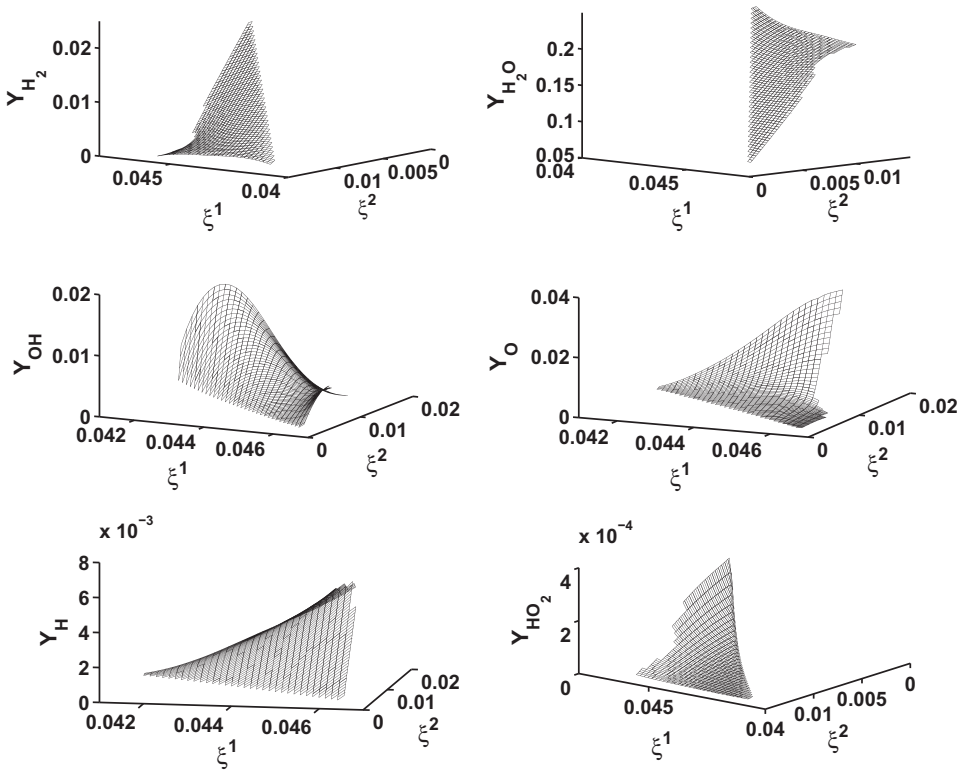

Fig. 2. Invariant grid approximating the slow invariant manifold.

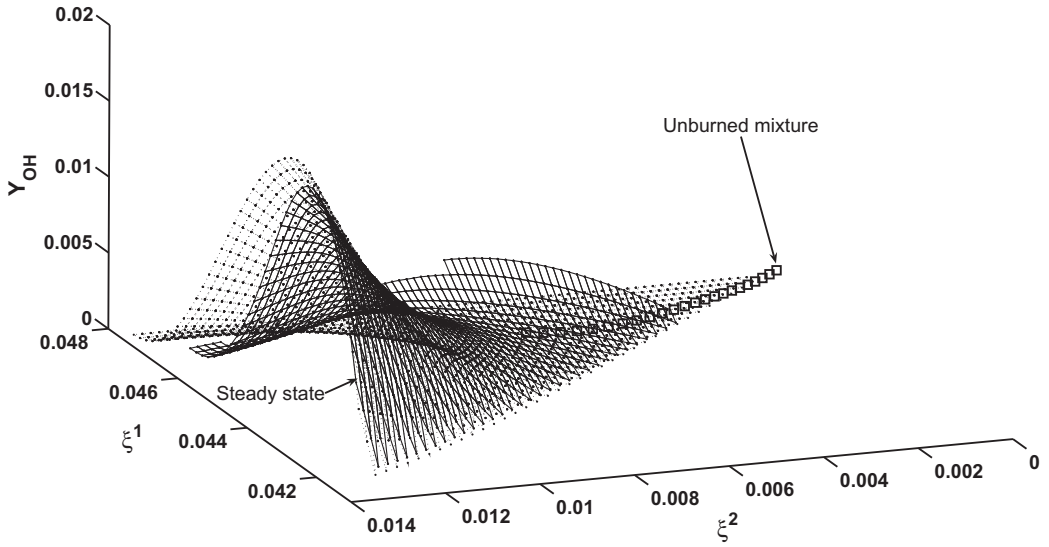

Fig. 3. OH coordinate: 2-dimensional quasi equilibrium grid (dashed lines), 2-dimensional invariant grid (continuous lines), trajectory starting from the unburned mixture (squares).

Remark. Notice that, in the example under study, the choice of a two-dimensional reduced system assumes a separation between the two slowest scales of the chemistry and the rest of the dynamics. Such an assumption is confirmed, at least in a neighborhood of the steady state $\boldsymbol{c}^{eq}$, by the following spectral analysis of the Jacobian matrix $\boldsymbol{J} = [\partial f_i/\partial Y_j]$ evaluated at $\boldsymbol{c}^{eq}$:

$$\begin{aligned} &\theta_1 \approx 2\times 10^{-4}, \quad \theta_2 \approx 7.7\times 10^{-6}, \quad \theta_3 \approx 4\times 10^{-7},\\ &\theta_4 \approx 2.5\times 10^{-7}, \quad \theta_5 \approx 2.2\times 10^{-7}, \quad \theta_6 \approx 1.5\times 10^{-7}, \end{aligned} \tag{19}$$

where the two time scales θ_1 and θ_2 (defined as the inverse of the non-zero eigenvalues of $\boldsymbol{J}$) are well separated from the others (θ_i, $i = 3, 4, 5, 6$). However, in the framework of the Method of Invariant Grid (MIG), the stability of the refinements, and hence the convergence of a solution toward a stable fixed point of the film Eq. (16), does provide a valuable indication of the existence of the slow invariant manifold (SIM) with a given dimension. Consequently, the convergence of the MIG algorithm (discussed in Section 3.2) demonstrates the validity of the above assumption concerning the dimension of the adopted reduced model, also in a large portion of the phase-space far from equilibrium. On the other hand, the lack of convergence of the MIG iterations in the low temperature domain ($T < 800$ K) denotes that here the dimension of the SIM q is larger than two. In this respect, it is worth stressing that only recently it has been possible to exploit the stability of solutions to the Eq. (16) for establishing a fully adaptive model reduction technique, where the dimension q of the SIM is automatically and consistently chosen without resorting to any *a-priori* assumptions [14]. Nevertheless, the latter issue is beyond the scope of the present work, whereas our main concern here is to show in full details the coupling of the MIG technique within the lattice Boltzmann method. Thus, for the sake of simplicity, in the low temperature domain, following others (see, e.g., [15,16]), we adopt a one-dimensional induction manifold obtained by a fit of a detailed solution of freely propagating flames trough hydrogen-air mixtures. The latter one-dimensional manifold is parameterized by the first reduced variable ξ^1 and, by starting from the fresh mixture composition, it bridges the gap between the unburned condition and the two-dimensional invariant grid.

3.3. Tabulation and interpolation

The grid coordinates, the thermodynamic projection of the vector field $\boldsymbol{f}$ and the two parameters ξ^1, ξ^2 are redistributed on a regular Cartesian grid, stored in two dimensional arrays and each grid node is identified by an index pair (i, j). Any tabulated quantity $\mathcal{Q}$, associated with a generic parameter pair (ξ^1, ξ^2), can be reconstructed by linear bi-variate interpolation:

$$\mathcal{Q} = \iota_A \mathcal{Q}_A + \iota_B \mathcal{Q}_B + \iota_C \mathcal{Q}_C + \iota_D \mathcal{Q}_D, \tag{20}$$

where A, B, C, D are the grid nodes corresponding to (i, j), $(i+1, j)$, $(i, j+1)$, $(i+1, j+1)$, respectively, while ι_A, ι_B, ι_C, ι_D are the interpolation weights

$$\begin{aligned} &\iota_A = (1-\pi_1)(1-\pi_2), \quad \iota_B = \pi_1(1-\pi_2),\\ &\iota_C = (1-\pi_1)\pi_2, \quad \iota_D = \pi_1\pi_2, \end{aligned} \tag{21}$$

with $\pi_1 = (\xi^1 - \xi^1_A)/(\xi^1_B - \xi^1_A)$ and $\pi_2 = (\xi^2 - \xi^2_A)/(\xi^2_C - \xi^2_A)$. Similar strategies of tabulation and interpolation are also used in other methods, such as the ILDM [35,18,19] and FGM [22,23].

3.4. Thermodynamic projector

It is important to discuss the projector $\boldsymbol{P}$ appearing in Eq. (16). MIG makes use of the *thermodynamic projector* [1], whose construction is briefly reviewed below. Let ∇G and T_ξ be the gradient of G and the tangent hyperplane, evaluated at a given grid node $\boldsymbol{c}$, respectively. Let $T_{\xi 0} = T_\xi \cap ker(\nabla G)$, where $ker(\nabla G)$ indicates the hyperplane orthogonal to ∇G. Assuming that $T_\xi \neq T_{\xi 0}$, let $\hat{\boldsymbol{u}}_1$ be a vector of the tangent plane T_ξ, such that $\nabla G \hat{\boldsymbol{u}}_1^T = 1$ and

$$\hat{\boldsymbol{u}}_1 \boldsymbol{H} \boldsymbol{x}^T = 0, \quad \boldsymbol{H} = \left[\frac{\partial^2 G}{\partial c_i \partial c_j}\right], \tag{22}$$

where $\boldsymbol{x}$ is an arbitrary vector of the subspace $T_{\xi 0}$. The thermodynamic projector acts on a generic vector $\boldsymbol{\eta}$ as follows

$$\boldsymbol{P}\boldsymbol{\eta} = (\boldsymbol{\eta}\nabla G^T)\hat{\boldsymbol{u}}_1 + \sum_{i=2}^{n} (\boldsymbol{\eta}\boldsymbol{H}\hat{\boldsymbol{u}}_i^T)\hat{\boldsymbol{u}}_i. \tag{23}$$

Here, the set of vectors $\{\hat{\boldsymbol{u}}_2, \ldots, \hat{\boldsymbol{u}}_n\}$ forms a basis of $T_{\xi 0}$, such that

$$\hat{\boldsymbol{u}}_i \boldsymbol{H} \hat{\boldsymbol{u}}_j^T = \delta_{ij}, \quad \forall i, j = 2, \ldots, n, \tag{24}$$

with δ_{ij} denoting the Kronecker delta. In the case $T_\xi = T_{\xi 0}$, let $\{\hat{\boldsymbol{u}}_1, \ldots, \hat{\boldsymbol{u}}_n\}$ be a basis of τ such that $\hat{\boldsymbol{u}}_i \boldsymbol{H} \hat{\boldsymbol{u}}_j^T = \delta_{ij}$, then (23) takes the form:

$$\boldsymbol{P\eta} = \sum_{i=1}^{n} (\boldsymbol{\eta H \hat{u}}_i^T)\hat{\boldsymbol{u}}_i. \tag{25}$$

It is worth noting here a remarkable feature of the thermodynamic projector: the construction of (23) or (25) performs slow-fast motion decomposition. In other words, in a neighborhood of an invariant grid, the slow dynamics of the kinetic Eq. (4) takes place in the image of $\boldsymbol{P}$, while the fast dynamics evolves in its null space. More details can be found in Refs. [1,6,12,8].

4. Lattice Boltzmann method for reactive flows

We consider here the simplest lattice Boltzmann formulation suitable for simulations of combustion. To this end, following the suggestion of Yamamoto et al. [25], reactive flows can be simulated with the lattice Boltzmann method as reported below. More elaborate and complete LB models for mixtures [27] and compressible flows [28] will be taken into account in the near future, too.

According to the standard terminology, LB schemes are usually denoted as *DMQN*, meaning that N particles move on a M-dimensional lattice. In Fig. 4, the most popular 2-dimensional lattice is shown, where each distribution function is represented by its own velocity $\boldsymbol{e}_\alpha$. In the following, we briefly review the LB algorithm with the BGK [30] collision model. A single-component fluid is described by a set of populations, which can be regarded as microscopic properties of the fluid. On the contrary, macroscopic quantities such as density and momentum (and also energy for thermal cases) are given by various moments of those populations. In terms of pressure distribution functions p_α, the LB equation takes the following discrete form at the lattice node $\boldsymbol{x}$:

$$p_\alpha(\boldsymbol{x}+\boldsymbol{e}_\alpha, t+\delta t) = p_\alpha(\boldsymbol{x},t) - \frac{1}{\tau_F}\left[p_\alpha(\boldsymbol{x},t) - p_\alpha^{eq}(p,\boldsymbol{u})\right], \tag{26}$$

where the equilibrium populations p_α^{eq} read:

$$p_\alpha^{eq} = w_\alpha \tilde{p}\left[1 + 3(\boldsymbol{e}_\alpha \boldsymbol{u}^T) + \frac{9}{2}(\boldsymbol{e}_\alpha \boldsymbol{u}^T)^2 - \frac{3}{2}\boldsymbol{u}^2\right]. \tag{27}$$

The pressure $\tilde{p}$ and the fluid velocity $\boldsymbol{u}$ are expressed in LB units (dimensionless), and are given by:

$$\tilde{p} = \sum_\alpha p_\alpha, \quad \boldsymbol{u} = \frac{1}{\tilde{p}_0}\sum_\alpha \boldsymbol{e}_\alpha p_\alpha, \tag{28}$$

where the reference pressure $\tilde{p}_0 = \tilde{\rho}_0/3$, with $\tilde{\rho}_0$ denoting the reference density of the LB model. Let δt be the time step, the relaxation parameter τ_F is related to the kinematic viscosity ν by (see, e.g., [34])

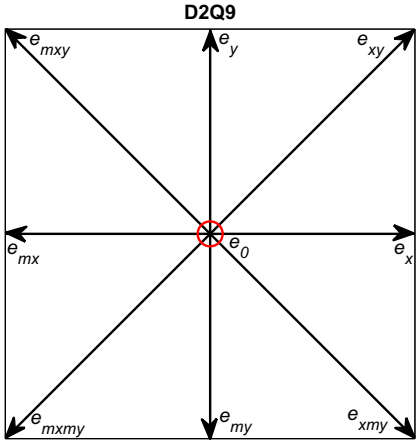

Fig. 4. 2-Dimensional 9-velocities lattice: *D2Q9*.

$$\nu = \frac{2\tau_F - 1}{6}\delta t. \tag{29}$$

In general, the discrete velocities can be regarded as the nodes of a Gauss–Hermite quadrature applied to the Maxwell–Boltzmann distribution function, and each of them is characterized by a proper weight w_α.

According to [25], the flow field in the present simplest LB model is not affected by the chemical reaction, transport coefficients are constant and Fick's law applies to the diffusion. In this case, the background flow is treated as a one-component medium whose pressure populations evolution obeys (26). Let $\bar{h}_0$ be a reference enthalpy, the evolution equations for enthalpy and concentration of species i are written as

$$\tilde{h}_\alpha(\boldsymbol{x}+\boldsymbol{e}_\alpha, t+\delta t) - \tilde{h}_\alpha(\boldsymbol{x},t) = -\frac{1}{\tau_h}\left[\tilde{h}_\alpha(\boldsymbol{x},t) - \tilde{h}_\alpha^{eq}(\tilde{h},\boldsymbol{u})\right] + w_\alpha Q_h, \tag{30}$$

$$Y_{i\alpha}(\boldsymbol{x}+\boldsymbol{e}_\alpha, t+\delta t) - Y_{i\alpha}(\boldsymbol{x},t) = -\frac{1}{\tau_{Y_i}}\left[Y_{i\alpha}(\boldsymbol{x},t) - Y_{i\alpha}^{eq}(Y_i,\boldsymbol{u})\right] + w_\alpha Q_{Y_i}, \tag{31}$$

where

$$\tilde{h} = \bar{h}^s/\bar{h}_0 = \sum_\alpha \tilde{h}_\alpha, \quad Y_i = \sum_\alpha Y_{i\alpha}, \tag{32}$$

and the equilibrium populations $\tilde{h}_\alpha^{eq}, Y_{i\alpha}^{eq}$ are expressed as in (27) after replacing $\tilde{p}$ with $\tilde{h}$ and Y_i, respectively. We notice that the Eq. (30) has been written in terms of the sensible enthalpy $\bar{h}^s$, which is linked to $\bar{h}$ by the caloric equation of state:

$$\bar{h} = \sum_{i=1}^{n} h_i(T)Y_i = \sum_{i=1}^{n} h_i^0(T)Y_i + \sum_{i=1}^{n} h_i^s(T)Y_i = \bar{h}^0 + \bar{h}^s, \tag{33}$$

with $\bar{h}^0$ denoting the chemical energy due to the species heats of formation, whereas the sensible (or thermal) enthalpy of species k can be expressed in terms of the heat capacity $C_{pk}(T)$ (at constant pressure) and reads:

$$h_k^s(T) = \int_0^T C_{pk}(T)dT. \tag{34}$$

Let t_0 be a factor for converting physical time into LB time units: $(t)_{LB} = (t)_{phys}/t_0$, the source terms take the explicit form

$$Q_h = \frac{1}{\bar{h}_0}\left(\sum_{i=1}^{9}\frac{\dot{\omega}_i W_i}{\bar{\rho}}h_i^0\right)t_0\delta t, \quad Q_{Y_i} = \frac{\dot{\omega}_i W_i}{\bar{\rho}}t_0\delta t, \tag{35}$$

where $\bar{\rho}$ is the mixture-averaged density (in physical units), while $\dot{\omega}_i$, W_i, h_i^0 denote the rate of change, molecular weight and enthalpy of formation of species i, respectively. The enthalpy Eq. (30) can also be written in terms of the mixture-averaged enthalpy $\bar{h}$. In this case, the latter equations have no source terms: $Q_h = 0$ and $\tilde{h} = \bar{h}/\bar{h}_0 = \sum_\alpha \tilde{h}_\alpha$. Similarly to (29), the thermal diffusivity κ and diffusion coefficient D_i of species i are related to the relaxation parameters as follows:

$$\kappa = \frac{2\tau_h - 1}{6}\delta t, \quad D_i = \frac{2\tau_{Y_i} - 1}{6}\delta t. \tag{36}$$

4.1. Discussion of the model

In the above section, we briefly reviewed the lattice Boltzmann model for reactive flows originally presented in [25], where more details can be found. However, it is worth reporting here the basic assumptions of the model:

- The chemical reaction does not affect the flow field in the incompressible model.
- The transport properties are constant.

- The diffusion follows the Fick's law.
- Viscous energy dissipation and radiative heat loss are neglected.

It is worth noticing that, the LB Eq. (26) for pressure density functions p_α recovers, in the low-Mach number regime, the incompressible Navier–Stokes equations, which can be written as follows (in the absence of body forces):

$$\partial_j u_j = 0$$
$$\partial_t u_i + u_j \partial_j u_i = -\frac{1}{\rho}\partial_i p + \partial_j(\nu \partial_j u_i). \tag{37}$$

Here, ∂_t and ∂_j denote partial derivatives with respect to time and the jth spacial direction respectively, while Einstein summation convention is adopted for j. Therefore, pressure and density only have small fluctuations around their reference values, and compressibility effects are not taken into account in this model. The above assumptions are adopted for the sake of simplicity, and the methodology of Section 4.2 can be used, in combination with more recent LB models where compressibility is included as well (see, e.g., [26]).

A detailed discussion on fundamental aspects of the lattice Boltzmann Eq. (26), derivation of the equilibrium populations (27), relations between transport coefficients and relaxation parameters (e.g., (29) and (36)) can be found in [31–34]. Moreover, the lattice Boltzmann Eqs. (30) and (31) simulate the following partial differential equations (PDE) [25]:

$$\partial_t \bar{h}^s + u_j \partial_j \bar{h}^s = \partial_j(\kappa \partial_j \bar{h}^s) + \sum_{i=1}^{n} \frac{\dot{\omega}_i W_i}{\bar{\rho}} h_i^0, \tag{38}$$

and

$$\bar{\rho}(\partial_t Y_i + u_j \partial_j Y_i) = \partial_j(\bar{\rho} D_i \partial_j Y_i) + \dot{\omega}_i W_i, \tag{39}$$

which account for the conservation of energy and a generic species i, respectively. We finally notice that, the utilized lattice Boltzmann scheme [25] only considers Fourier heat flux in the enthalpy Eq. (38) (no relative enthalpy fluxes).

4.2. Lattice Boltzmann and reduced model

In the following, in order to reduce the complexity of the validation procedure, we use the assumption of equal diffusivity $D_i = D$ and Lewis number $Le = \kappa/D = 1$ for all chemical species. In this case, the mixture enthalpy $\bar{h}$ and the element compositions N_k in (11) remain constant throughout the domain, thus the reduced dynamics takes place along a single invariant grid constructed under fixed pressure, mixture-averaged enthalpy at stoichiometric proportions. As discussed in more detail below, the latter assumption is not restricting and a fully general case can be handled by extending the invariant grid with enthalpy, pressure and element compositions as additional degrees of freedom, in the same spirit as the ILDM [35,18,19] method is applied to similar problems. On the other hand, in premixed systems, element fractions are often conserved up to small fluctuations and, for such applications, only pressure and enthalpy are needed as new grid parameters. Finally, in combustion problems with low-Mach number, the pressure p can be considered constant for most cases (isobaric assumption [24]). The species Eq. (31) describe transport phenomena (diffusion and convection) in addition to the chemical reactions. On the other hand, by construction, the reduced models of Section 3 deliver invariant grids under the dynamics of the only chemical source terms. The basic assumption of the suggested procedure for reducing chemical kinetics (with n degrees of freedom) is that a generic state $\boldsymbol{c}$ is (at any time and at any point in space) close to an attractive *chemical* low dimensional manifold (of dimension $q \ll n$). Therefore, the reactive system admits a significant simplification by assuming that all states are confined to those manifolds and are function of a few independent variables only. In other words, we assume that transport phenomena only act as small perturbations rapidly relaxing toward the above invariant (with respect to the chemistry) manifolds. Therefore, a coupling of the flow solver and the reduced combustion model can be achieved by projecting the dynamics due to transport onto the slow subspace (see also the ILDM strategy [35]). Here, for projection purposes, it proves convenient to assume (following the rationale behind the quasi equilibrium manifold) that the fixed parameterization vectors $\boldsymbol{m}_j$ (approximately) globally span the slow subspace (see e.g., the RCCE ans SQE parameterization discussed in Section 3.1). In fact, a projection of the species Eq. (39) onto the latter slow subspace yields:

$$\bar{\rho}(\partial_t \xi^j + u_\alpha \partial_\alpha \xi^j) = \partial_\alpha(\bar{\rho} D \partial_\alpha \xi^j) + \sum_{i=1}^{n} m_j^i \dot{\omega}_i W_i, \tag{40}$$

which is recovered by the following lattice Boltzmann equations in terms of the slow variables ξ^j:

$$\xi_\alpha^j(\boldsymbol{x} + \boldsymbol{e}_\alpha, t + \delta t) - \xi_\alpha^j(\boldsymbol{x}, t) = -\frac{1}{\tau_\xi}[\xi_\alpha^j(\boldsymbol{x}, t) - \xi_\alpha^{jeq}(\xi^j, \boldsymbol{u})] + w_\alpha Q_{\xi^j}. \tag{41}$$

Here, the equilibrium populations for the reduced variables ξ^j read

$$\xi_\alpha^{jeq} = w_\alpha \xi^j \left[1 + 3(\boldsymbol{e}_\alpha \boldsymbol{u}^T) + \frac{9}{2}(\boldsymbol{e}_\alpha \boldsymbol{u}^T)^2 - \frac{3}{2}\boldsymbol{u}^2\right], \tag{42}$$

where $D = \delta t(2\tau_\xi - 1)/6, Q_{\xi^j} = \sum_i m_j^i Q_{Y_i}, \xi^j = \sum_{i=1}^{9} m_j^i Y_i = \sum_{\alpha=1}^{3} \xi_\alpha^j$. Now, simulations can be carried out by solving for only the two lumped variables ξ^j using Eq. (41) and tabulated source terms Q_{ξ^j}, while the flow dynamics still obeys (26). Computation results are expressed in terms of slow variables ξ^j, while other relevant fields $Y_i(\xi^1,\xi^2)$, $T(\xi^1,\xi^2)$ can be reconstructed by interpolation on the invariant grid in a post-processing as described in Section 3.3.

Remark. In the case of low-Mach number combustion and fixed pressure [24], the above assumptions can be gradually relaxed, so that three cases of different complexity are obtained.

1. Equal diffusivities with $Le = 1$. Even though this might lead to an inaccurate approximation for hydrogen systems (e.g., quite different diffusivities should be used for light species such as H_2 and H), here it is considered for validation purposes. Moreover, such a condition is of interest for simulating turbulent flames [37].
2. Equal diffusivities with $Le \neq 1$. In this case, the element composition is conserved but the mixture-averaged enthalpy $\bar{h}$ changes in the domain. Now, the conservation equation for enthalpy (30) has to be solved along with (41), and the reduced system is fully described by three variables: ξ^1, ξ^2 and $\bar{h}$ (three dimensional grid). Hence, the construction of Section 3 has to be performed for a discrete set of enthalpies.
3. General case. In general, also the element composition varies in the domain due to differential diffusion effects. Thus, equations for the lumped variables ξ^j, mixture enthalpy $\bar{h}$ and the element mole numbers N_k need to be solved, whereas a generic tabulated quantity is function of additional variables: $\mathcal{Q} = \mathcal{Q}(\xi^1, \xi^2, \bar{h}, \mathrm{N_H}, \mathrm{N_O}, \mathrm{N_N})$. Now, a projection of the species Eq. (39) onto the slow subspace spanned by $\boldsymbol{m}_j$ gives:

$$\bar{\rho}(\partial_t \xi^j + u_\alpha \partial_\alpha \xi^j) = \partial_\alpha(\bar{\rho} D^j \partial_\alpha \xi^j) + \sum_{i=1}^{n} m_j^i \dot{\omega}_i W_i + \partial_\alpha(\bar{\rho} \xi^j \partial_\alpha D^j), \tag{43}$$

where an *effective diffusion coefficient* D^j of the slow variable ξ^j can be defined as follows:

$$D^j = \sum_{i=1}^{n} D_i m_j^i Y_i \Big/ \sum_{i=1}^{n} m_j^i Y_i. \tag{44}$$

Moreover, the evolutionary equation for the element mole number N_k is obtained from (11) and (39):

$$\bar{\rho}(\partial_t N_k + u_j \partial_j N_k) = \partial_j \left(\bar{\rho} \partial_j \left(\sum_{i=1}^{n} \frac{D_i \mu_{ik} Y_i}{W_i} \right) \right), \tag{45}$$

where

$$N_k = \sum_{i=1}^{n} \frac{\mu_{ik} Y_i}{W_i}.$$

For mass is conserved, the contribution due to the source terms $\dot{\omega}_i$ vanishes in (45). Formula (45) can be recast as follows:

$$\bar{\rho}(\partial_t N_k + u_j \partial_j N_k) = \partial_j(\bar{\rho} \overline{D}_k \partial_j N_k) + Q_{N_k}, \quad Q_{N_k} = \partial_j(\bar{\rho} N_k \partial_j \overline{D}_k) \tag{46}$$

where the quantities

$$\overline{D}_k = \left(\sum_{i=1}^{n} \frac{D_i \mu_{ik} Y_i}{W_i} \right) \Big/ \sum_{i=1}^{n} \frac{\mu_{ik} Y_i}{W_i}, \tag{47}$$

and D^j (44) can be also tabulated as functions of the grid parameters. Notice that, both Eqs. (43) and (46) present the same form as the species Eq. (39) with diffusivity D^j and $\overline{D}_k$, respectively and non-local source terms. Therefore, the latter partial differential equations can be still solved using a lattice Boltzmann type Eq. (31) with a variable relaxation parameter and the extra source terms approximated e.g., with finite differences (see Section 4.6).

4.3. Example: premix counterflow flames

Here, we consider the so-called counterflow laminar flame as a two dimensional benchmark of the suggested methodology. A well premixed stoichiometric H_2-air mixture is uniformly ejected from two parallel stationary flat nozzles, located at $y = \pm L_y$. When properly ignited, the fuel reacts generating two twin flames in this counterflow, while the burned gas exits the domain along the x-direction. As illustrated in the sketch of Fig. 5, under the assumption of symmetrical flow with respect to the symmetry lines $x = 0$ mm and $y = 0$ mm, the computational domain can be restricted to the region where $x \geqslant 0$ mm and $y \geqslant 0$ mm, and simulations can be carried out using the standard 2-dimensional lattice $D2Q9$ by detailed and reduced models. In both cases, the mixture, initially under room temperature $T_0 = 300$ K, is ignited by placing a hot spot at the origin of the reference system.

In the present configuration, the half-length of the gap between the two nozzles is $L_y = 2$ mm, the computational domain is rectangular with aspect-ratio $L_x/L_y = 1.67$, and symmetry conditions at the stagnation lines are used. At the inlet, we impose a constant velocity $u_{in} = -2.4$ m/s, room temperature $T_{in} = 300$ K, pressure $p = p_0 = 1$ bar and species concentrations corresponding to the unburned mixture. At the outlet, the pressure is constant $p = p_0$, and we utilize fully developed boundary conditions as discussed below.

Notice that, all quantities given in physical units of time (s) and length (m) are converted into LB units dividing by the factors

$$t_0 = \frac{\left(\frac{L_y}{u_{in}}\right)_{phys}}{\left(\frac{L_y}{u_{in}}\right)_{LB}}, \quad L_0 = \frac{(L_y)_{phys}}{(L_y)_{LB}}, \tag{48}$$

respectively. Let δy be the space step along the y direction, the time step

$$\delta t_{LB} = \left(\frac{\delta y}{e}\right)_{LB}, \quad \delta t_{phys} = t_0 \delta t_{LB}, \tag{49}$$

is set by defining the ratio $(L_y/u_{in})_{LB}$, and $e = 1$ is the magnitude of the intermediate non-zero lattice velocities ($\boldsymbol{e}_x$, $\boldsymbol{e}_{mx}$, $\boldsymbol{e}_y$, $\boldsymbol{e}_{my}$) of Fig. 4.

4.4. Flow field

In our simulation, we adopt a $200(N_x) \times 120(N_y)$ grid, and a constant kinematic viscosity: $\nu = 1.6 \times 10^{-5}$ m^2/s. At the inlet, the equilibrium populations, corresponding to the pressure $p = p_0 = 1$ bar and velocities $u_x = 0, u_y = u_{in}$, are maintained. In order to implement symmetry condition, we apply the *mirror bounce-back* scheme to the missing pressure density functions along the stagnation line $x = 0$ mm:

$$p_x = p_{mx}, \quad p_{xy} = p_{mxy}, \quad p_{xmy} = p_{mxmy}, \tag{50}$$

while along the line $y = 0$ mm,

$$p_y = p_{my}, \quad p_{xy} = p_{xmy}, \quad p_{mxy} = p_{mxmy}. \tag{51}$$

At the outlet, fully developed boundary conditions are imposed by replacing all pressure populations with the corresponding equilibrium populations evaluated with $p = p_0$ and velocities at the neighbor node along x:

$$p_\alpha(N_x) = p_\alpha^{eq}(p_0, u_x(N_x - 1), u_y(N_x - 1)). \tag{52}$$

Finally, the wall of the nozzle at the end of the upper limit of the domain is simulated using five nodes, where the *usual bounce-back* condition is imposed:

$$p_{my} = p_y, \quad p_{xmy} = p_{mxy}, \quad p_{mxmy} = p_{xy}. \tag{53}$$

It has been proved that the lattice Boltzmann method is able to reproduce the results of conventional methods (finite differences) in the case of counterflow with high accuracy [25]. Figure 6 shows the streamlines of the flow field when the steady solution is reached, while in Fig. 7 we report the normalized velocities (with respect to u_{in}) along the stagnation lines.

4.5. Temperature and concentration fields

In the following, we compute the temperature and concentration fields using both the detailed and reduced (two degrees of freedom) models. For the sake of simplicity, here we assume equal diffusion coefficients $D_i = D = 5 \times 10^{-5}$ m^2/s for all species, and unity Lewis number: $Le = D/\kappa = 1$. In this case, the two-dimensional invariant grid of Fig. 3 can be adopted as reduced description of the detailed model. According to the procedure of Section 4.2, here we apply the lattice Boltzmann equation only to the grid parameters $\xi^{1,2}$ (13), while species mass fractions and temperature field are reconstructed in a post-processing via bi-linear interpolation on the grid. Notice however that, the invariant grid does not extend in the low-temperature region of the phase-space. Therefore, instead of detailed chemistry, a 1-dimensional induction manifold is used. The latter manifold (squares in Fig. 3) is obtained by a fit from a detailed solution in the case of 1-dimensional freely propagating flame trough a stoichiometric homogeneous mixture of hydrogen and air.

Similarly to the pressure populations, the mirror bounce-back scheme is used as boundary condition for the missing density functions, $Y_{i,\alpha}, \xi_\alpha^i$, along the stagnation lines. At the inlet, the equilibrium populations corresponding to the unburned mixture are constantly imposed, while at the outlet we make use of the following extrapolation:

$$Y_{i\alpha}(N_x) = Y_{i\alpha}(N_x - 1), \quad \xi_\alpha^i(N_x) = \xi_\alpha^i(N_x - 1), \tag{54}$$

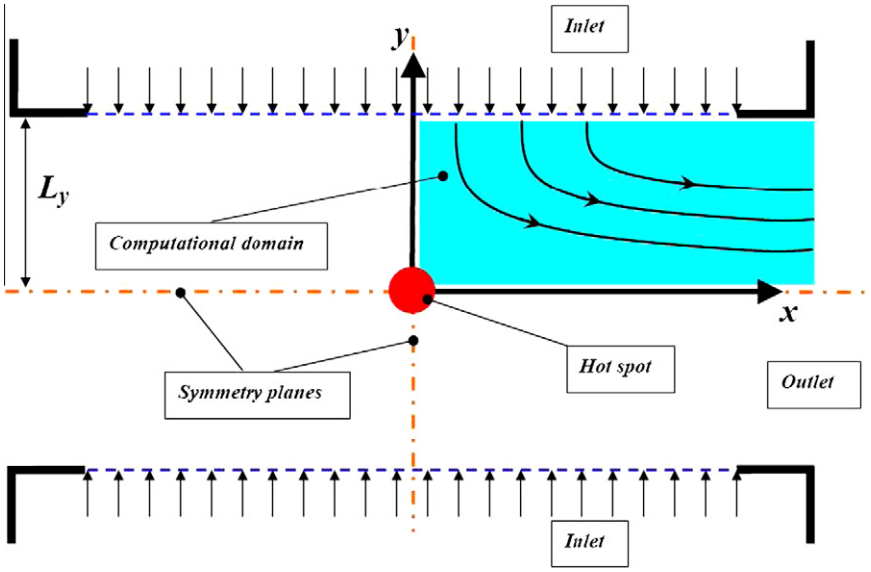

Fig. 5. Schematic representation of the 2-dimensional counterflow setup.

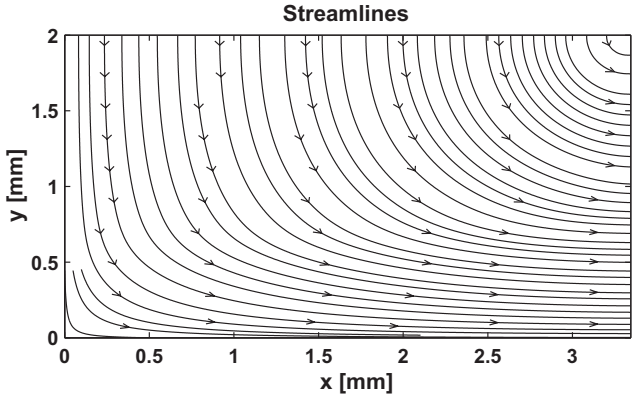

Fig. 6. Streamlines of the background flow field.

for the detailed and reduced model, respectively. The nozzle wall is supposed to be adiabatic and the usual bounce-back condition is adopted. Because of unity Lewis number, the mixture-averaged enthalpy $\bar{h}$ remains constant in the entire domain, thus it is dependent on the species concentrations through the uppermost equation in (9).

The hydrogen-air mixture, initially under room temperature $T_0 = 300$ K, is ignited by placing a hot spot at the origin of the reference system. A comparison between the detailed and reduced fields, along two lines ($x = 0$ mm and $x = 2.16$ mm) at two time instants ($t = 0.42$ ms and $t = 1.05$ ms) is shown in Figs. 8–10, and an excellent agreement is demonstrated. Moreover, in Figs. 11–14 we report sequences of snapshots where the mass fraction of the *OH* radical and the temperature field are shown, according to both the detailed and reduced model, in the whole computational domain.

On the basis of the present study, we can argue that the reduced model is indeed able to match the detailed solution with high accuracy. However, due to the reduced stiffness of the dynamics along the invariant grid, the time step δt needed for stably solving the lattice Boltzmann equations can be increased by an order of magnitude in the reduced model. In particular, the computation of the reduced solution, carried out by means of a 2 GHz Intel Core 2 Duo CPU, requires around 1 h per 1 ms simulation, whereas the computation of the detailed solution requires around 2 days ($\approx$ 48 h) per 1 ms simulation.

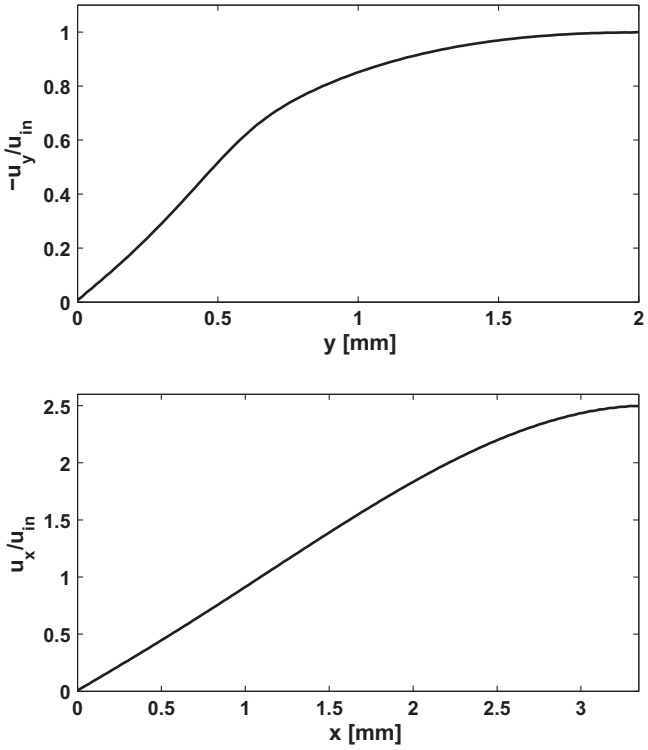

Fig. 7. Distribution of non-dimensional velocities along the symmetry axis.

4.6. Summary of the suggested procedure

For the sake of clarity, below we further illustrate all the steps involved in the construction of a reduced model and its implementation in a lattice Boltzmann flow solver. In Section 3, we discuss the construction of a simplified model (described by q independent parameters ξ^i) of an homogeneous reactive mixture in a closed system under fixed mixture-averaged enthalpy $\bar{h}$ an pressure p, whose detailed description requires $n - d > q$ degrees of freedom. The latter task is accomplished by computation of a discrete

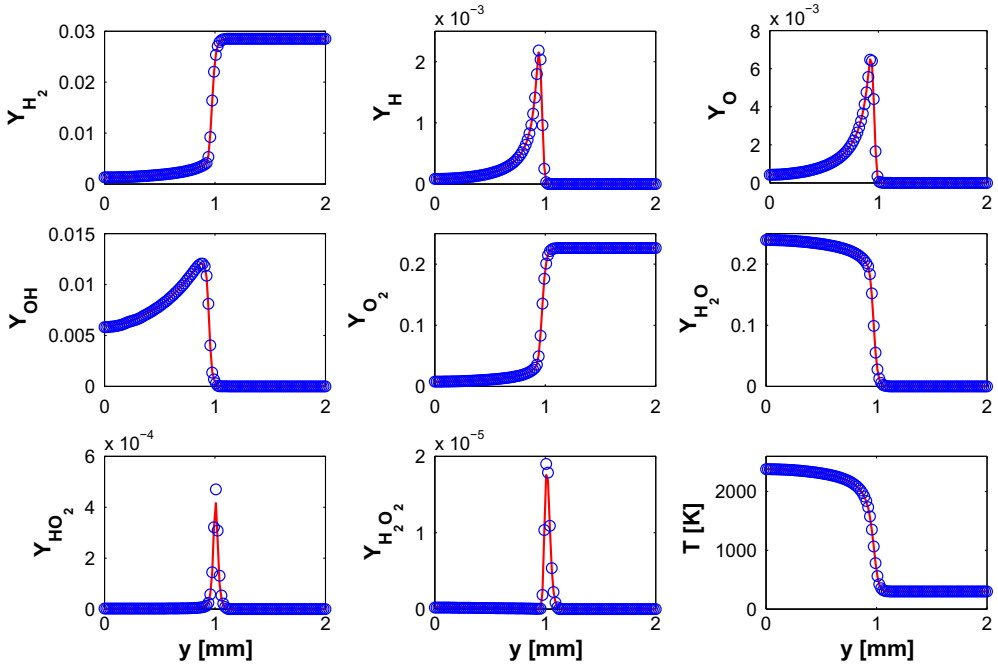

Fig. 8. Comparison between detailed (line) and reduced (circles) concentration and temperature profiles along the stagnation line $x = 0$ mm at the fixed time instant $t = 1.05$ ms.

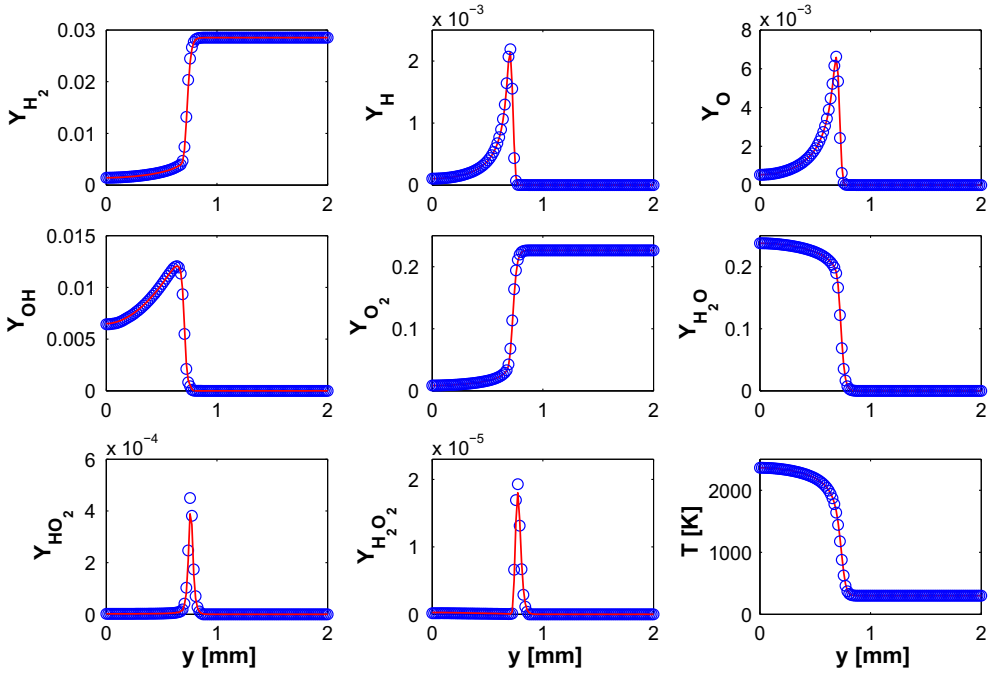

Fig. 9. Comparison between detailed (line) and reduced (circles) concentration and temperature profiles along the stagnation line $x = 0$ mm at the fixed time instant $t = 0.42$ ms.

approximation of the quasi equilibrium manifold (i.e. a quasi equilibrium grid [6]) and subsequent refinement according to the numerical scheme (17), with the aim of finding the stable fixed point of the film equation of dynamics (16). The above procedure can be summarized by means of the following *pseudo-algorithm*:

1. Start from full system of kinetic Eq. (9) of dimension $n - d$.
2. Find steady state.
3. If a SQE-manifold [7] is to be constructed, compute Jacobian matrix at steady state (e.g., by the exact formula (85) in Appendix B) and find the q slowest left eigenvectors.
4. Else use the RCCE parameterization (e.g., total number of moles, free oxygen, etc.) [10,11].
5. Construct the initial QE-grid according to the system (14) supplemented by the formulas in Appendix A for the derivatives of G.

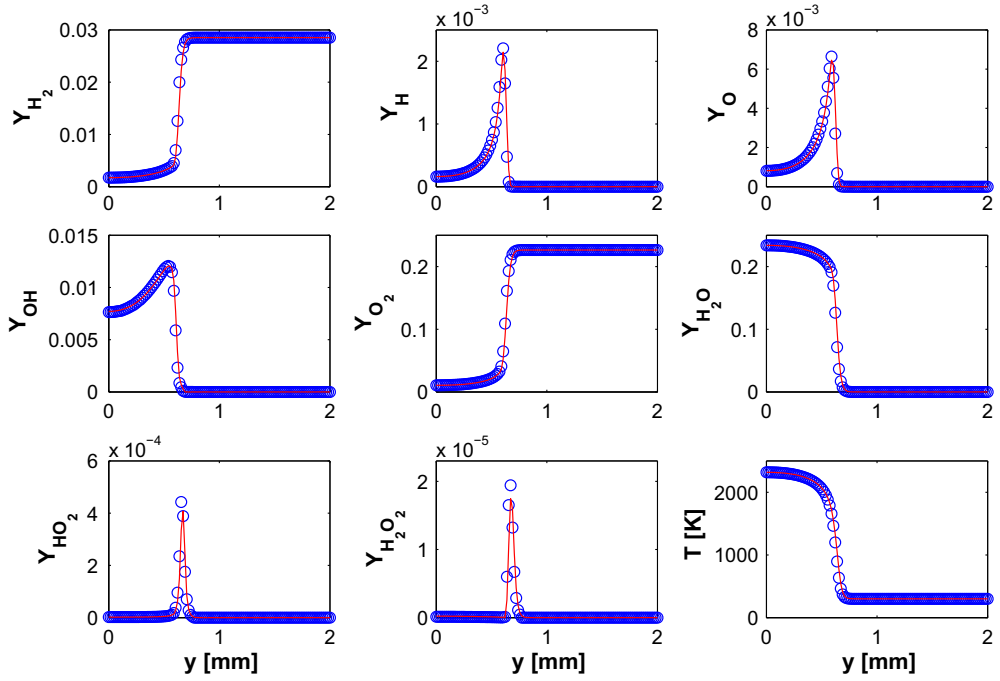

Fig. 10. Comparison between detailed (line) and reduced (circles) concentration and temperature profiles along the line $x = 2.16$ mm at the fixed time instant $t = 0.42$ ms.

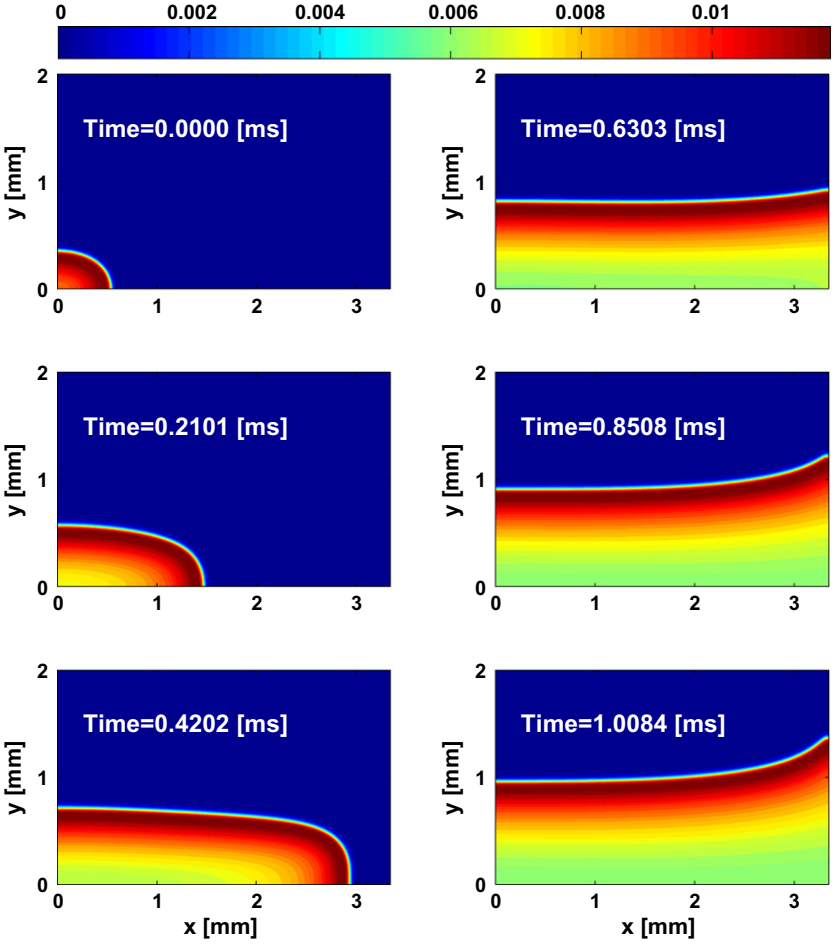

Fig. 11. Detailed model using the *D2Q9* lattice in combination with a 2-dimensional invariant grid: evolution of the mass fraction of OH radical.

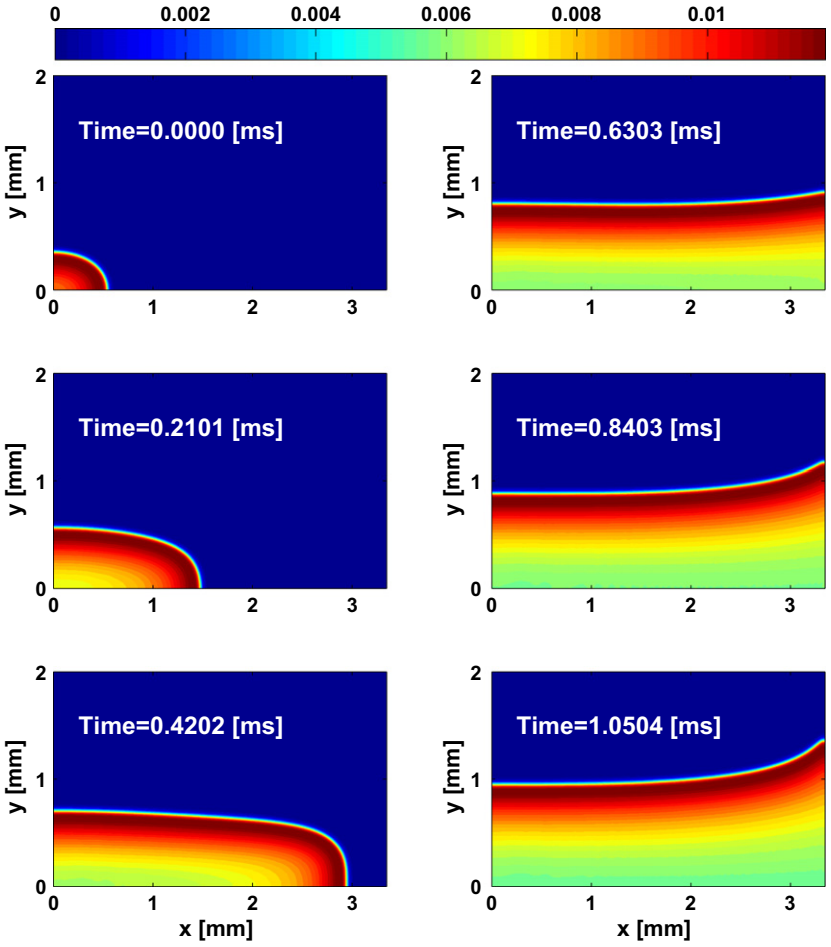

Fig. 12. Reduced model using the *D2Q9* lattice in combination with a 2-dimensional invariant grid: evolution of the mass fraction of OH radical.

6. Compute the q tangent vectors at any grid node by finite differences.
7. Compute both the vector field $\boldsymbol{f}$ and its local projection $\boldsymbol{Pf}$ according to the thermodynamic projector (23) (∇G and $\boldsymbol{H}$ are explicitly reported in Appendix A).
8. Correct each grid node according to (17).
9. Compare norm of invariance defect vs norm of vector field: $|\boldsymbol{\Delta}|/|\boldsymbol{f}|$.
10. If $|\boldsymbol{\Delta}|/|\boldsymbol{f}|$ is larger than a threshold then go to 6.

Upon convergence of the above algorithm, the q grid parameters ξ^i and the invariant grid coordinates can be stored in tables along with their rates:

$$\frac{d\xi^i}{dt} = \boldsymbol{m}_i \boldsymbol{P}\boldsymbol{f}. \tag{55}$$

It is worth stressing that, although the chosen parameterization vectors $\boldsymbol{m}_i$ affect the accuracy of the QE-manifold, the invariant grid delivered by the subsequent refinement is anyway a remarkably accurate description of the corresponding SIM (see, e.g., [2,7]). Importantly, the reduced stiffness in the rates (55) is ensured by the thermodynamic projector $\boldsymbol{P}$ (23) since the fast component of $\boldsymbol{f}$: $\boldsymbol{f}^{fast}$ belong to the null space of $\boldsymbol{P}$ [12]:

$$\boldsymbol{P}\boldsymbol{f}^{fast} = 0. \tag{56}$$

Toward the end of coupling such reduced models within a flow solver, in the same spirit of other techniques (e.g., ILDM [35,17]), the above algorithm is to be performed over a range of enthalpies $\bar{h}$ and element mole numbers N_k (for low-Mach number problems, we may invoke the isobaric assumption [24]). Thus, in general, all tabulated quantities $\mathscr{Q}$ depend on q chemical variables ξ^i, the mixture-averaged enthalpy $\bar{h}$ and d element mole numbers N_k : $\mathscr{Q} = \mathscr{Q}(\xi^i, \bar{h}, N_k)$. Namely, in a reduced model, only the evolutionary equations for the latter independent variables are to be solved. In particular, the set of governing equations of the reduced description is formed by (26), (30) conveniently written in terms of the mixture-averaged enthalpy $\bar{h}$ in addition to the equations recovering (43) and (46):

$$\xi^j_\alpha(\boldsymbol{x}+\boldsymbol{e}_\alpha, t+\delta t) - \xi^j_\alpha(\boldsymbol{x}, t) = -\frac{1}{\tau_j}\left[\xi^j_\alpha(\boldsymbol{x}, t) - \xi^{jeq}_\alpha(\xi^j, \boldsymbol{u})\right] + w_\alpha\left(Q_{\xi^j} + Q'_j\right), \tag{57}$$

$$N_{k\alpha}(\boldsymbol{x}+\boldsymbol{e}_\alpha, t+\delta t) - N_{k\alpha}(\boldsymbol{x}, t) = -\frac{1}{\tau_{N_k}}\left[N_{k\alpha}(\boldsymbol{x}, t) - N^{eq}_{k\alpha}(N_k, \boldsymbol{u})\right] + w_\alpha Q_{N_k}, \tag{58}$$

where

$$N_k = \sum_\alpha N_{k\alpha}, \quad \overline{D}^j = \frac{2\tau_j - 1}{6}\delta t, \quad \overline{D}_k = \frac{2\tau_{N_k} - 1}{6}\delta t, \tag{59}$$

with D^j and $\overline{D}_k$ given by (44) and (47) respectively, while the non-local source terms $Q'_j = \partial_\alpha(\bar{\rho}\xi^j\partial_\alpha\overline{D}^j)$, $Q_{N_k} = \partial_\alpha(\bar{\rho}N_k\partial_\alpha\overline{D}_k)$ can be estimated by finite differences. Notice that a reduced stiffness of the Eqs. (41) and (57) is achieved by imposing the chemical source terms:

$$Q_{\xi^j} = \frac{d\xi^i}{dt}, \tag{60}$$

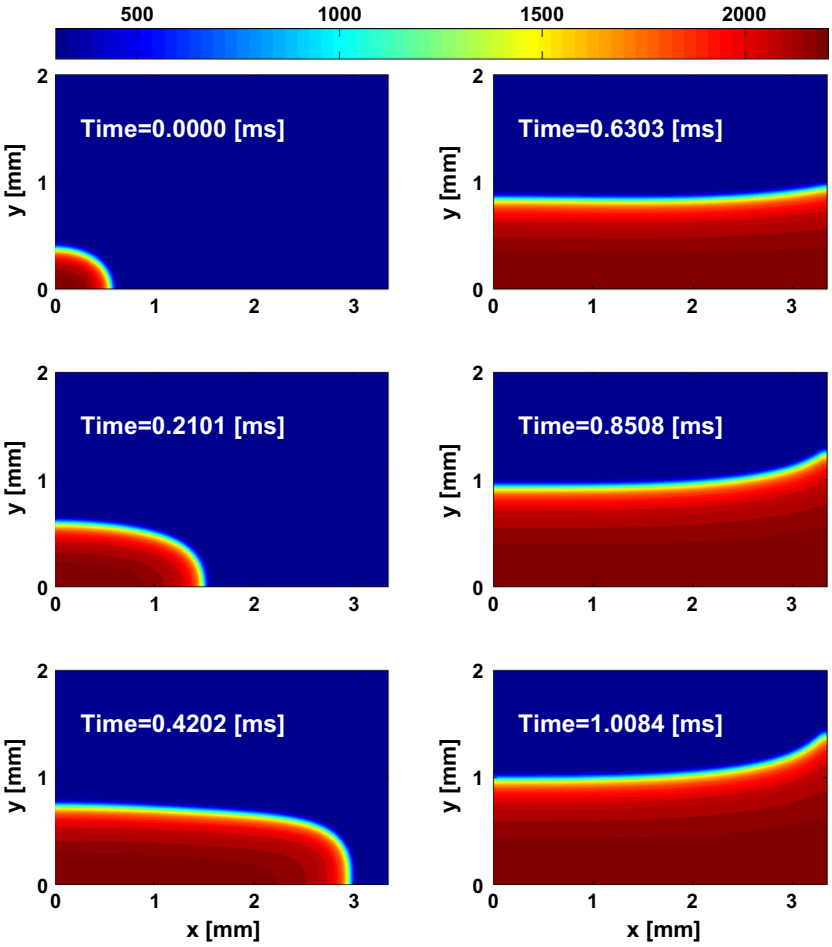

Fig. 13. Detailed model using the *D2Q9* lattice in combination with a 2-dimensional invariant grid: evolution of the temperature field.

according to (55). As discusses above in the Section 4.2, under the simplifying assumptions of equal diffusivities for all the chemical species and unity Lewis number (typically done in turbulent combustion), the number of table entries (hence of governing equations to solve) can be reduced to $(\xi^i, \bar{h})$ and ξ^i, respectively.

We stress that, instead of the global method described in Section 3 where invariant grids are pre-computed in the entire phase-space, tabulated and used at a later time, as an alternative, local approaches can be adopted since their coupling in the presented framework is straightforward. In particular, the recently suggested local construction of invariant grids [13,14], circumvents the issue of storage and interpolation of relatively high dimensional tables, by a local closure of the set of reduced governing Eqs. (26), (30), (57) and (58). In other words, any quantity $\mathcal{Q} = \mathcal{Q}(\xi^i, \bar{h}, N_k)$ can be obtained by targeting the construction of the invariant grid in the small region of the phase-space only when required in the simulation. In general, the coupling of a reduced model for combustion within a lattice Boltzmann flow solver can be schematically summarized by the following pseudo-algorithm:

1. Initialize the Eqs. (26), (30), (57) and (58).
2. Compute all source terms $\mathcal{Q} = \mathcal{Q}(\xi^i, \bar{h}, N_k)$ by interpolation on pre-computed table or, as an alternative, by local construction of the invariant grid [13,14].
3. Integrate the Eqs. (26), (30), (57) and (58).
4. Go back to 2 until convergence.
5. Post-processing for computing all fields of interest.

Finally, the efficiency of local model reduction approaches can be remarkably improved when used in combination with storage-retrieval methodologies such as *in situ* adaptive tabulation (ISAT) [20,21].

5. Discussion

In this paper, we suggested a methodology for using accurate reduced chemical kinetics in combination with a lattice Boltzmann solver for simulating reactive flows. It has been shown that the method of invariant grids (MIG) is suitable for providing the reduced description of chemistry, and this approach enables to cope with stiffness when solving the species equations. This is particularly desirable in the case of explicit solvers, and it results in a remarkable speedup due to the possibility of choosing a larger time step δt.

Moreover, the number of fields involved in the computation is drastically reduced, and this aspect is of paramount importance because it effectively addresses the issue of large memory demand. Indeed, while simulating reactive flows with detailed chemistry by the lattice Boltzmann method, the number of fields (density functions) stored in memory is remarkably large compared to conventional methods by a factor ranging from tens to hundreds in the case of 2- and 3-dimensional problems. Therefore, for instance, detailed LB simulations of 2- and 3-dimensional hydrocarbon flames (with hundreds of chemical species) are currently not affordable. In that respect, the present study intends to be a first step toward the

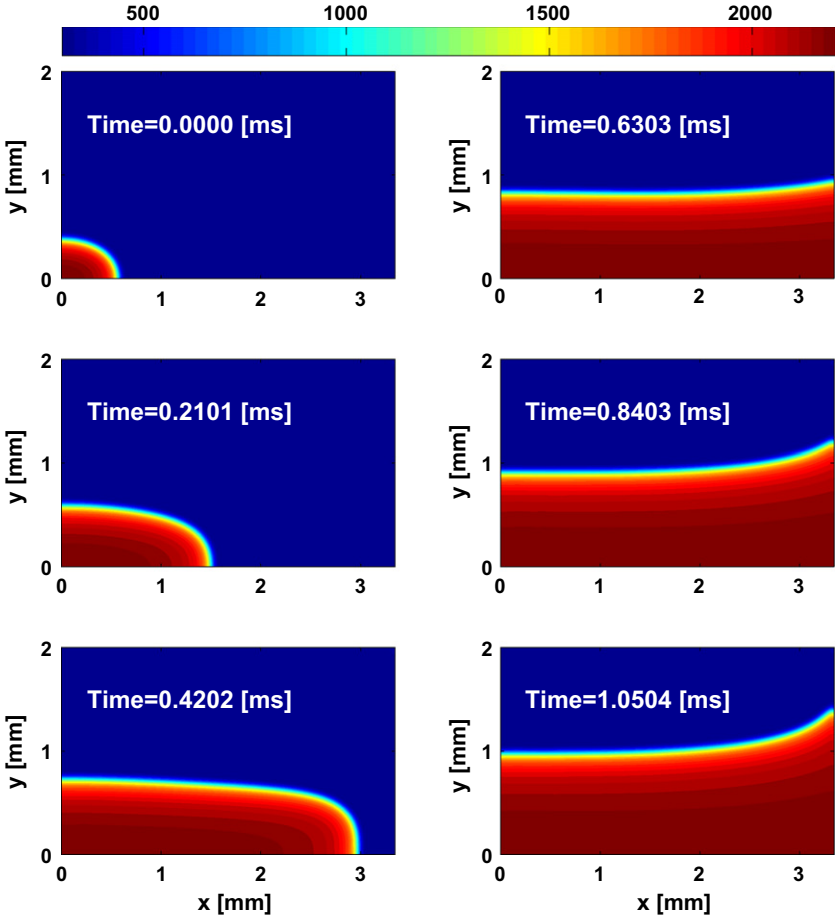

Fig. 14. Reduced model using the *D2Q9* lattice in combination with a 2-dimensional invariant grid: evolution of the temperature field.

efficient, yet accurate, solution to this problem. Applications with hydrocarbon fuels (e.g., methane) and more sophisticated LB models, capable to take into account compressibility effects, shall be considered in the near future.

The construction of thermodynamic Lyapunov functions G for reactive mixtures under non-isothermal conditions, the exact computation of the derivatives of G and Jacobian matrix are presented in an exhaustive manner with the help of two appendixes. Those are important details concerning the construction of quasi equilibrium grids, the construction of thermodynamic projector and implementation of the method of invariant grid.

Finally, notice that the method of invariant grids is a general technique for model reduction of chemical kinetics, and it can be still adopted together with different flow solvers, not necessarily based on the lattice Boltzmann method.

Acknowledgments

This work was accomplished under the financial support of Swiss National Science Foundation (SNF, Project 200021-107885/1) and CCEM-CH.

Appendix A

In Section 2, we assume that the reaction kinetic Eq. (4), together with a proper closure, describe the temporal evolution of a closed reactive system towards a unique steady state. In particular, there are two classical conditions relevant to combustion applications:

1. isobaric isenthalpic system;
2. isolated system.

Due to the second law of thermodynamics, for those cases there exists a strictly convex function, only dependent on the state, that decreases monotonically in time under the dynamics dictated by the kinetic equations. Such a function is a global Lyapunov function with respect to the governing Eq. (4), and it reaches its global minimum at the steady state. In particular, for both isobaric isenthalpic mixtures and isolated systems, the thermodynamic Lyapunov function G can be constructed on the basis of the specific mixture-averaged entropy $\bar{s}$ (in mass units) as follows:

$$G = -\bar{s} + \sum_{k=1}^{d} \left(\lambda_k \sum_{i=1}^{n} \frac{\mu_{ik}}{W_i} Y_i \right), \tag{61}$$

where the evaluation of the Lagrange multipliers λ_k is discussed below, and $\bar{s}$ takes the explicit form:

$$\bar{s} = \frac{1}{\overline{W}} \sum_{i=1}^{n} \left[s_i(T) - \mathscr{R} \ln(X_i) - \mathscr{R} \ln\left(\frac{p}{p_{ref}} \right) \right] X_i. \tag{62}$$

The mixture mean molecular weight $\overline{W}$ and the mole fraction X_k can be expressed in terms of mass fractions as

$$\overline{W} = \frac{1}{\sum_{j=1}^{n} Y_j / W_j}, \quad X_k = \frac{Y_k}{W_k \sum_{j=1}^{n} Y_j / W_j}. \tag{63}$$

The specific entropy s_j of species j depends on the temperature T as follows:

$$s_j(T) = \mathscr{R}\left(a_{1j}\ln T + a_{2j}T + \frac{a_{3j}}{2}T^2 + \frac{a_{4j}}{3}T^3 + \frac{a_{5j}}{4}T^4 + a_{7j}\right), \tag{64}$$

and p_{ref} represents a reference pressure, which generally is assumed to be 1 bar. Computing the gradient ∇G and the Hessian matrix $\boldsymbol{H}$ in the phase-space is not straightforward, since (61) explicitly depends on the temperature, which is in turn implicit function of $\bar{h}$ or $\overline{U}$ through the non-linear relations in (8) and (10). In our study, three approaches have been implemented and tested. The first approach is named *finite differencing*, and it approximates the exact first derivative (e.g., for isobaric isenthalpic systems) by the following ratio:

$$\left.\frac{\partial G}{\partial c_i}\right|_{p,\bar{h}} \cong \frac{G(T',\ldots,c_i+\varepsilon,\ldots) - G(T,\ldots,c_i,\ldots)}{\varepsilon}, \tag{65}$$

with the temperature T' evaluated by solving (e.g. iteratively by Newton–Raphson method) the following equation:

$$\bar{h}(T',\ldots,c_i+\varepsilon,\ldots) = \bar{h}(T,\ldots,c_i,\ldots). \tag{66}$$

In general, first derivatives are evaluated using either forward (such as (65)) or backward approximations, while central schemes are preferred for second derivatives. Moreover, in order to improve the accuracy, the positive small parameter ε must be chosen of the order of the square root of machine precision. More details can be found e.g., in [38].

Alternatively, it is possible to differentiate (in principle up to any order) the subroutine itself which evaluates the function (61): such a technique is known as *automatic differentiation* (AD). In the case of systems with fixed $\bar{h}$ and p, the AD was applied to the main subroutine implementing (61), where the temperature is given by a secondary subroutine implementing a Newton–Raphson method for solving the enthalpy conservation equation in (10). The AD systematically applies the chain rule to the full sequence of elementary assignments in the code, and it provides with exact values of the derivatives, which are thus not affected by any round-off errors (unlike the finite differencing). However, by using the code INTLAB [39] for Matlab, we have found that the AD is slower than the finite differencing by one order of magnitude.

Finally, it is possible to find the exact form of the derivatives of G, and in the following we illustrate this approach for an isobaric isenthalpic reactor. The mixture-averaged specific enthalpy for an ideal mixture is

$$\bar{h}(T,Y_i) = \sum_{i=1}^{n} h_i(T)Y_i, \tag{67}$$

and the total differential $d\bar{h}$ takes the form:

$$d\bar{h}(T,Y_i) = \left.\frac{\partial \bar{h}}{\partial T}\right|_{Y_i} dT + \left.\frac{\partial \bar{h}}{\partial Y_1}\right|_{T,Y_{i\neq 1}} dY_1 + \cdots + \left.\frac{\partial \bar{h}}{\partial Y_n}\right|_{T,Y_{i\neq n}} dY_n. \tag{68}$$

Setting $d\bar{h} = 0$ (isenthalpic system), and recording the definition of mixture-averaged specific heat under constant pressure $\overline{C}_p$ and specific enthalpies h_i, the exact differential of temperature is written as:

$$dT = -\frac{1}{\overline{C}_p(T,Y_1,\ldots,Y_n)}\sum_{i=1}^{n} h_i(T)dY_i. \tag{69}$$

In other words, the partial derivatives of temperature under constant pressure and mixture-averaged specific enthalpy read:

$$\left.\frac{\partial T}{\partial Y_i}\right|_{p,\bar{h}} = -\frac{h_i(T)}{\overline{C}_p(T,Y_1,\ldots,Y_n)} = -\frac{h_i(T)}{\sum_{j=1}^{n} C_{pj}(T)Y_j}, \tag{70}$$

where the fit for the specific heat C_{pj} of species j takes the form [42]

$$C_{pj}(T) = \mathscr{R}(a_{1j} + a_{2j}T + a_{3j}T^2 + a_{4j}T^3 + a_{5j}T^4). \tag{71}$$

The derivative of (70), with respect to Y_j, reads

$$\left.\frac{\partial^2 T}{\partial Y_i \partial Y_j}\right|_{p,\bar{h}} = \frac{h_i(T)C_{pj}(T)}{\overline{C}_p^2(T,Y_1,\ldots,Y_n)} - \frac{h_i(T)h_j(T)}{\overline{C}_p^3(T,Y_1,\ldots,Y_n)}\sum_{k=1}^{n} Y_k\frac{dC_{pk}}{dT}(T). \tag{72}$$

By making use of the relations (63) and the chain rule, it is now possible to write explicitly the components of the gradient ∇G,

$$\left.\frac{\partial G}{\partial Y_i}\right|_{p,\bar{h}} = -\frac{s_i}{W_i} - \left.\frac{\partial T}{\partial Y_i}\right|_{p,\bar{h}}\sum_{k=1}^{n}\frac{Y_k}{W_k}\frac{ds_k}{dT} + \frac{\mathscr{R}}{W_i}\ln\left(\frac{Y_i\overline{W}}{W_i}\right) + \frac{\mathscr{R}}{W_i}\times\ln\left(\frac{p}{p_{ref}}\right) + \sum_{k=1}^{d}\lambda_k\frac{\mu_{ik}}{W_i}, \tag{73}$$

and of the Hessian matrix $\boldsymbol{H}$,

$$\left.\frac{\partial^2 G}{\partial Y_i \partial Y_j}\right|_{p,\bar{h}} = \frac{-1}{W_i}\frac{ds_i}{dT}\left.\frac{\partial T}{\partial Y_j}\right|_{p,\bar{h}} - \frac{1}{W_j}\frac{ds_j}{dT}\left.\frac{\partial T}{\partial Y_i}\right|_{p,\bar{h}} - \left.\frac{\partial^2 T}{\partial Y_i \partial Y_j}\right|_{p,\bar{h}}\sum_{k=1}^{n}\frac{Y_k}{W_k}\frac{ds_k}{dT} - \left.\frac{\partial T}{\partial Y_i}\right|_{p,\bar{h}}\left.\frac{\partial T}{\partial Y_j}\right|_{p,\bar{h}}\sum_{k=1}^{n}\frac{Y_k}{W_k}\frac{d^2 s_k}{dT^2} + \frac{\mathscr{R}}{W_i}\left(\frac{\delta_{ij}}{Y_i} - \frac{\overline{W}}{W_j}\right), \tag{74}$$

with δ_{ij} denoting the Kronecker delta.

Let us assume that the steady state of the system has been computed (e.g., using STANJAN [41]). Let $\partial G^*/\partial Y_i$ be the first derivative of G, at the steady state, evaluated by setting $\lambda_k = 0$, $k = 1,\ldots,d$, in (73). Imposing the following zero-gradient condition at the steady state (point of global minimum):

$$\begin{bmatrix} \frac{\mu_{11}}{W_1} & \cdots & \frac{\mu_{1d}}{W_d} \\ \vdots & \ddots & \vdots \\ \frac{\mu_{n1}}{W_1} & \cdots & \frac{\mu_{nd}}{W_d} \end{bmatrix}\begin{bmatrix} \lambda_1 \\ \vdots \\ \lambda_d \end{bmatrix} = -\begin{bmatrix} \frac{\partial G^*}{\partial Y_1} \\ \vdots \\ \frac{\partial G^*}{\partial Y_n} \end{bmatrix}, \tag{75}$$

and applying the first Gauss transformation to the rectangular algebraic system (75), the condition for the Lagrange multipliers λ_k is explicitly written:

$$\begin{bmatrix} \frac{\mu_{11}}{W_1} & \cdots & \frac{\mu_{1d}}{W_d} \\ \vdots & \ddots & \vdots \\ \frac{\mu_{n1}}{W_1} & \cdots & \frac{\mu_{nd}}{W_d} \end{bmatrix}^T\begin{bmatrix} \frac{\mu_{11}}{W_1} & \cdots & \frac{\mu_{1d}}{W_d} \\ \vdots & \ddots & \vdots \\ \frac{\mu_{n1}}{W_1} & \cdots & \frac{\mu_{nd}}{W_d} \end{bmatrix}\begin{bmatrix} \lambda_1 \\ \vdots \\ \lambda_d \end{bmatrix} = -\begin{bmatrix} \frac{\mu_{11}}{W_1} & \cdots & \frac{\mu_{1d}}{W_d} \\ \vdots & \ddots & \vdots \\ \frac{\mu_{n1}}{W_1} & \cdots & \frac{\mu_{nd}}{W_d} \end{bmatrix}^T\begin{bmatrix} \frac{\partial G^*}{\partial Y_1} \\ \vdots \\ \frac{\partial G^*}{\partial Y_n} \end{bmatrix}.$$

The case of an isolated system ($\overline{U}, V = const$) can be analyzed in a similar manner. This time, the partial derivatives (70) and (72) can be written as:

$$\left.\frac{\partial T}{\partial Y_i}\right|_{V,\overline{U}} = -\frac{U_i(T)}{\overline{C}_v(T,Y_1,\ldots,Y_n)} = -\frac{U_i(T)}{\sum_{j=1}^{n} C_{vj}(T)Y_j},$$

$$\left.\frac{\partial^2 T}{\partial Y_i \partial Y_j}\right|_{V,\overline{U}} = \frac{e_i(T)C_{vj}(T)}{\overline{C}_v^2(T,Y_1,\ldots,Y_n)} - \frac{U_i(T)U_j(T)}{\overline{C}_v^3(T,Y_1,\ldots,Y_n)}\sum_{k=1}^{n} Y_k\frac{dC_{vk}}{dT}(T),$$

where $\overline{C}_v$ is the mixture-averaged specific heat under constant volume, and $C_{vj}(T)$, for any species j, is given by the Meyer relation:

$$C_{vj} = C_{pj} - \mathscr{R}.$$

Moreover, now the mixture density $\bar{\rho}$ is constant while the pressure

$$p = \bar{\rho}\mathscr{R}T\sum_{i=1}^{n}\frac{Y_i}{W_i}$$

changes in time, and this needs to be taken into account in formulas (73) and (74).

Notice however that, it proves convenient to describe isolated reacting mixtures in terms of molar concentrations c_i. Indeed, since the mixture density $\bar{\rho} = \sum_{i=1}^{n} W_i c_i$ is now both a conserved quantity and a linear combination of molar concentrations, it can be used for constructing the Lyapunov function G as follows:

$$G = -\bar{s} + \sum_{k=1}^{d}\left(\lambda_k\sum_{i=1}^{n}\mu_{ki}c_i\right) + \lambda\sum_{i=1}^{n}W_i c_i. \tag{76}$$

Thus, it suffices to compute all derivatives under fixed $\overline{U}$, and their explicit expressions are derived below. The conservation of the mixture-averaged internal energy can be written

$$\overline{C}_v dT + \frac{1}{\bar{\rho}}\sum_{k=1}^{n}W_k U_k(T)dc_k = 0,$$

so that the first and second partial derivatives of temperature with respect to molar concentrations take the form:

$$\left.\frac{\partial T}{\partial c_i}\right|_{\overline{U}} = -\frac{W_i U_i(T)}{\bar{\rho}\overline{C}_v}, \tag{77}$$

$$\left.\frac{\partial^2 T}{\partial c_j \partial c_i}\right|_{\overline{U}} = -\frac{W_i\left(\overline{C}_v\left.\frac{dU_i}{dT}\frac{\partial T}{\partial c_j}\right|_{\overline{U}} - U_i\left.\frac{\partial \overline{C}_v}{\partial c_j}\right|_{\overline{U}}\right)}{\bar{\rho}\overline{C}_v^2}, \tag{78}$$

where

$$\overline{C}_v = \frac{1}{\bar{\rho}}\sum_{k=1}^{n}W_k C_{vk}(T)c_k, \left.\frac{\partial \overline{C}_v}{\partial c_j}\right|_{\overline{U}} = \frac{1}{\bar{\rho}}\left[\left.\frac{\partial T}{\partial c_j}\right|_{\overline{U}}\left(\sum_{k=1}^{n}W_k\frac{dC_{vk}}{dT}c_k\right) + W_j C_{vj}(T)\right].$$

By definition, mole fractions and molar concentrations are related by

$$mix = \sum_{j=1}^{n}c_j, \quad X_k = \frac{c_k}{mix},$$

so that the following condition holds:

$$\frac{\partial X_k}{\partial c_i} = \frac{\delta_{ki}mix - c_k}{mix^2}. \tag{79}$$

The gradient of the G function (76) has the following components:

$$\left.\frac{\partial G}{\partial c_i}\right|_{\overline{U}} = -\frac{1}{\bar{\rho}}\left[\left.\frac{\partial T}{\partial c_i}\right|_{\overline{U}}\left(\sum_{k=1}^{n}\frac{ds_k}{dT}c_k\right) + s_i\right] + \frac{\mathscr{R}}{\bar{\rho}}\ln\left(\frac{c_i}{\sum_{k=1}^{n}c_k}\right) + \frac{\mathscr{R}}{\bar{\rho}}\left[\ln\left(\frac{p}{p_{ref}}\right) + \frac{\sum_{k=1}^{n}c_k\left.\frac{\partial p}{\partial c_i}\right|_{\overline{U}}}{p}\right] + \sum_{k=1}^{d}\lambda_k\mu_{ik} + \lambda W_i, \tag{80}$$

where

$$p = \mathscr{R}T\sum_{k=1}^{n}c_k, \quad \left.\frac{\partial p}{\partial c_i}\right|_{\overline{U}} = \mathscr{R}\left.\frac{\partial T}{\partial c_i}\right|_{\overline{U}}\sum_{k=1}^{n}c_k + \mathscr{R}T,$$

while the Hessian matrix of G is computed as follows:

$$\left.\frac{\partial^2 G}{\partial c_j \partial c_i}\right|_{\overline{U}} = -\frac{1}{\bar{\rho}}\left.\frac{\partial^2 T}{\partial c_j \partial c_i}\right|_{\overline{U}}\left(\sum_{k=1}^{n}\frac{ds_k}{dT}c_k\right) - \frac{1}{\bar{\rho}}\left.\frac{\partial T}{\partial c_i}\right|_{\overline{U}}\left.\frac{\partial T}{\partial c_j}\right|_{\overline{U}}\left(\sum_{k=1}^{n}\frac{d^2 s_k}{dT^2}c_k\right) - \frac{1}{\bar{\rho}}\left.\frac{\partial T}{\partial c_i}\right|_{\overline{U}}\frac{ds_j}{dT} - \frac{1}{\bar{\rho}}\left.\frac{\partial T}{\partial c_j}\right|_{\overline{U}}\frac{ds_i}{dT} + \frac{\mathscr{R}}{\bar{\rho}}\frac{\sum_{k=1}^{n}c_k}{c_i}\frac{\partial X_i}{\partial c_j} + \frac{\mathscr{R}}{\bar{\rho}}\left[\frac{1}{p}\left(\left.\frac{\partial p}{\partial c_j}\right|_{\overline{U}} + \left.\frac{\partial p}{\partial c_i}\right|_{\overline{U}}\right) - \frac{\sum_{k=1}^{n}c_k}{p^2}\left.\frac{\partial p}{\partial c_j}\right|_{\overline{U}}\left.\frac{\partial p}{\partial c_i}\right|_{\overline{U}} + \frac{1}{\mathscr{R}T}\left.\frac{\partial^2 p}{\partial c_j \partial c_i}\right|_{\overline{U}}\right], \tag{81}$$

and the second derivative matrix of pressure reads

$$\left.\frac{\partial^2 p}{\partial c_j \partial c_i}\right|_{\overline{U}} = \mathscr{R}\left(\left.\frac{\partial^2 T}{\partial c_j \partial c_i}\right|_{\overline{U}}\sum_{k=1}^{n}c_k + \left.\frac{\partial T}{\partial c_i}\right|_{\overline{U}} + \left.\frac{\partial T}{\partial c_j}\right|_{\overline{U}}\right).$$

The Lagrange multipliers λ_k and λ in (80) are derived in a similar way as illustrated for the previous case, by imposing zero gradient at the steady state.

Finally, we should stress that, due to the second law of thermodynamics, (61) and (76) represent two *global* Lyapunov functions with respect to the kinetic systems (9) and (7), respectively. The condition (75) is imposed at the equilibrium point $\boldsymbol{c}^{eq}$, and it is adopted only to identify the Lagrange multipliers λ_k such that the zero-gradient condition is fulfilled at $\boldsymbol{c}^{eq}$ (consistently with the Lyapunov second theorem on stability). Therefore, the above expressions are general and can be adopted in the entire phase-space for implementing the quasi equilibrium grid algorithm (14), constructing the thermodynamic projector (23), and computing the *exact* Jacobian matrix $\boldsymbol{J}$ as reported below in Appendix B. Toward this end, only the coefficients a_{ji} (readily available from the Chemkin databases [42]) in the expressions (8), (64) and (71) are required for each chemical species involved in a complex reaction.

Appendix B

Let $\boldsymbol{\psi}$ be an arbitrary point of the phase-space. The linearization of the vector field of motion $\boldsymbol{f}$ about $\boldsymbol{\psi}$ is written:

$$\boldsymbol{f}(\boldsymbol{\psi} + \delta\boldsymbol{\psi}) \cong \boldsymbol{f}(\boldsymbol{\psi}) + \boldsymbol{J}(\boldsymbol{\psi})\delta\boldsymbol{\psi}, \tag{82}$$

where the Jacobian matrix $\boldsymbol{J} = [\partial f_i/\partial Y_j]$ can be related to the Hessian matrix $\boldsymbol{H} = [\partial^2 G/\partial Y_i\,\partial Y_j]$ of the Lyapunov function G, and it acts on an arbitrary vector $\boldsymbol{\eta}$ as follows:

$$\boldsymbol{J}\boldsymbol{\eta}^T = \sum_{s=1}^{r}\boldsymbol{\nu}_s\left[\Omega_s^+(\boldsymbol{\alpha}_s\boldsymbol{H}\boldsymbol{\eta}^T) - \Omega_s^-(\boldsymbol{\beta}_s\boldsymbol{H}\boldsymbol{\eta}^T)\right]. \tag{83}$$

The matrix $\boldsymbol{J}$ in (83) can be decomposed as shown below:

$$\boldsymbol{J} = \boldsymbol{J}' + \boldsymbol{J}'', \tag{84}$$

where the two matrices $\boldsymbol{J}'$ and $\boldsymbol{J}''$ act as follows:

$$\boldsymbol{J}'\boldsymbol{\eta}^T = -\frac{1}{2}\sum_{s=1}^{r}\left[\Omega_s^+ + \Omega_s^-\right]\boldsymbol{\nu}_s(\boldsymbol{\nu}_s\boldsymbol{H}\boldsymbol{\eta}^T), \tag{85}$$

$$\boldsymbol{J}''\boldsymbol{\eta}^T = \frac{1}{2}\sum_{s=1}^{r}\left[\Omega_s^+ - \Omega_s^-\right]\boldsymbol{\nu}_s\left((\boldsymbol{\alpha}_s + \boldsymbol{\beta}_s)\boldsymbol{H}\boldsymbol{\eta}^T\right). \tag{86}$$

The Jacobian decomposition (84) splits $\boldsymbol{J}$ in two parts. The first one $\boldsymbol{J}'$ is symmetric in the following sense

$$\boldsymbol{\eta}_1\boldsymbol{J}'\boldsymbol{H}\boldsymbol{\eta}_2^T = \boldsymbol{\eta}_2\boldsymbol{J}'\boldsymbol{H}\boldsymbol{\eta}_1^T, \quad \forall\boldsymbol{\eta}_1, \boldsymbol{\eta}_2, \tag{87}$$

while the second one $\boldsymbol{J}''$ vanishes at the steady state, due to the principle of detail balance: $\Omega_s^+ = \Omega_s^-$. In other words, at the steady state of the system, we have

$$\boldsymbol{J} = \boldsymbol{J}'. \tag{88}$$

The symmetric part $\boldsymbol{J}'$ is relevant to the MIG method, and it takes the following explicit form:

$$\sum_{j=1}^{n} \boldsymbol{J}'(i,j)\boldsymbol{\eta}(j) = -\sum_{s=1}^{r} \frac{\Omega_s^+ + \Omega_s^-}{2} \boldsymbol{v}_s(i) \sum_{j=1}^{n} (\boldsymbol{H}\boldsymbol{v}_s^T)(j)\boldsymbol{\eta}(j),$$

$$\sum_{j=1}^{n} \boldsymbol{J}'(i,j)\boldsymbol{\eta}(j) = -\sum_{s=1}^{r} \sum_{j=1}^{n} \frac{\Omega_s^+ + \Omega_s^-}{2} \boldsymbol{v}_s(i)(\boldsymbol{H}\boldsymbol{v}_s^T)(j)\boldsymbol{\eta}(j),$$

$$\sum_{j=1}^{n} \boldsymbol{J}'(i,j)\boldsymbol{\eta}(j) = -\sum_{j=1}^{n} \sum_{s=1}^{r} \frac{\Omega_s^+ + \Omega_s^-}{2} \boldsymbol{v}_s(i)(\boldsymbol{H}\boldsymbol{v}_s^T)(j)\eta(j),$$

$$\boldsymbol{J}'(i,j) = -\sum_{s=1}^{r} \frac{\Omega_s^+ + \Omega_s^-}{2} \boldsymbol{v}_s(i)(\boldsymbol{H}\boldsymbol{v}_s^T)(j). \tag{89}$$

Similarly, the non symmetric part of the Jacobian matrix $\boldsymbol{J}''$ can be written as follows:

$$\boldsymbol{J}''(i,j) = \sum_{s=1}^{r} \frac{\Omega_s^+ - \Omega_s^-}{2} \boldsymbol{v}_s(i)[\boldsymbol{H}(\boldsymbol{\alpha}_s + \boldsymbol{\beta}_s)^T](j). \tag{90}$$

Remark. Notice that, any function obtained by multiplying G in (61) and (76) by an arbitrary factor is still a thermodynamic Lyapunov function with respect to the kinetic equations. Therefore, the matrices $\boldsymbol{J}$, $\boldsymbol{J}'$ and $\boldsymbol{J}''$ can be analytically determined, up to an unknown multiplicative constant, using (84), (89), (90) and the explicit expressions for $\boldsymbol{H}$ described in Appendix A. Nevertheless, if needed, the unknown multiplicative constant can be recovered by computing the Jacobian $\boldsymbol{J}$ via automatic differentiation only at the steady state, and imposing the equality condition (88).

References

[1] A. Gorban, I.V. Karlin, Invariant Manifolds for Physical and Chemical Kinetics, Springer, Berlin, 2005.
[2] A.N. Gorban, I.V. Karlin, A.Y. Zinovyev, Physica A 333 (2004) 106–154.
[3] A.N. Gorban, I.V. Karlin, Chem. Eng. Sci. 58 (2003) 4751–4768.
[4] J. Li, Z. Zhao, A. Kazakov, F.L. Dryer, Int. J. Chem. Kinet. 36 (2004) 566–575.
[5] Q. Tang, S.B. Pope, Combust. Theo. Model. 8 (2004) 255–279.
[6] E. Chiavazzo, I.V. Karlin, J. Comput. Phys. 227 (2008) 5535–5560.
[7] E. Chiavazzo, A.N. Gorban, I.V. Karlin, Commun. Comput. Phys. 2 (2007) 964–992.
[8] E. Chiavazzo, I.V. Karlin, C.E. Frouzakis, K. Boulouchos, Proc. Combust. Inst. 32 (2009) 519–526.
[9] E. Chiavazzo, I.V. Karlin, A.N. Gorban, K. Boulouchos, J. Stat. Mech. (2009) P06013.
[10] J.C. Keck, D. Gillespie, Combust. Flame 17 (1971) 237–241.
[11] P.S. Bishnu, D. Hamiroune, M. Metghalchi, J.C. Keck, Combust. Theo. Model. 1 (1997) 295.
[12] E. Chiavazzo, I.V. Karlin, A.N. Gorban, Commun. Comput. Phys. 8 (2010) 701–734.
[13] E. Chiavazzo, Invariant Manifolds and Lattice Boltzmann for Combustion. PhD thesis, Swiss Federal Institute of Technology, ETH-Zurich, 2009, pp. 100–106.
[14] E. Chiavazzo, I.V. Karlin, preprint (2010).
[15] C.A. Eckett, Numerical and Analytical Studies of the Dynamics of Gaseous Detonations. PhD thesis, California Institute of Technology, Pasadena California, 2001, pp. 128–133.
[16] P. Hung, Algorithms for Reaction Mechanism Reduction and Numerical Simulation of Detonations Initiated by Projectiles. PhD thesis, California Institute of Technology, Pasadena California, 2003, p. 86.
[17] V. Bykov, U. Maas, Proc. Combust. Inst. 31 (2007) 465–472.
[18] B. Fiorina, R. Baron, O. Gicquel, D. Thevenin, S. Carpentier, N. Darabiha, Combust. Theo. Model. 7 (2003) 449–470.
[19] V. Bykov, U. Maas, Combust. Theo. Model. 11 (2007) 839–862.
[20] B. Yang, S.B. Pope, Combust. Flame 112 (1998) 85–112.
[21] S.B. Pope, Combust. Theo. Model. 1 (1997) 41.
[22] J.A. van Oijen, F.A. Lammers, L.P.H. de Goey, Combust. Flame 127 (2001) 2124–2134.
[23] A.W. Vreman, B.A. Albrecht, J.A. van Oijen, L.P.H. de Goey, R.J.M. Bastiaans, Combust. Flame 153 (2008) 394–416.
[24] C.K. Law, Combustion Physics, Cambridge University Press, 2006. 168–169.
[25] K. Yamamoto, X. He, G.D. Doolen, J. Stat. Phys. 107 (2002) 367–383.
[26] S. Chen, Z. Liu, Z. Tian, B. Shi, C. Zheng, Comput. Math. Appl. 55 (2008) 1424–1432.
[27] S. Arcidiacono, I.V. Karlin, J. Mantzaras, C.E. Frouzakis, Phys. Rev. E 76 (2007) 046703.
[28] N. Prasianakis, I.V. Karlin, Phys. Rev. E 76 (2007) 016702.
[29] S.S. Chikatamarla, C.E. Frouzakis, I.V. Karlin, A.G. Tomboulides, K.B. Boulouchos, J. Fluid Mech. (2010).
[30] P.L. Bhatnagar, E.P. Gross, M. Krook, Phys. Rev. 94 (3) (1954) 511–525.
[31] S. Succi, The Lattice Boltzmann Equation for Fluid Dynamics and Beyond, Oxford University Press, Oxford, 2001.
[32] I.V. Karlin, A. Ferrante, H.C. Öttinger, Europhys. Lett. 47 (2) (1999) 182–188.
[33] S. Ansumali, I.V. Karlin, H.C. Öttinger, Europhys. Lett. 63 (6) (2003) 798–804.
[34] S. Chen, G. Doolen, Annu. Rev. Fluid Mech. 30 (1998) 329–364.
[35] U. Maas, S.B. Pope, Combust. Flame 88 (1992) 239–264.
[36] S.H. Lam, D.A. Goussis, Int. J. Chem. Kinet. 26 (1994) 461–486.
[37] P.A. Libby, F.A. Williams (Eds.), Turbulent Reactive Flows, Springer, New York, 1980.
[38] G. Buzzi Ferraris, Metodi Numerici e Software in C++, Pearson Education Italia, 1998.
[39] S.M. Rump, in: T. Csendes (Ed.), Kluwer Academic Publischers, Dordrecht, 1999, pp. 77–104.
[40] F.A. Williams, Combustion Theory, Addison-Wesley Publishing Company, 1985.
[41] W.C. Reynolds, The Element Potential Method for Chemical Equilibrium Analysis, Mechanical Engineering Department, Standford University, 1986.
[42] R.J. Kee, G. Dixon-Lewis, J. Warnatz, M.E. Coltrin, J.A. Miller, Report No. SAND86-8246, Sandia National Laboratories, 1996.